CRYSTAL GROWTH & DESIGN

pubs.acs.org/crystal

Review

Kinking in Semiconductor Nanowires: A Review

Sergei Vlassov,* Sven Oras, Boris Polyakov, Edgars Butanovs, Andreas Kyritsakis, and Veronika Zadin

Cite This: *Cryst. Growth Des.* 2022, 22, 871−892

Read Online

ACCESS | Metrics & More | Article Recommendations

ABSTRACT: The growth direction of nanowires (NWs) can change during synthesis as a result of stochastic processes or modulation of certain growth conditions. This phenomenon is known as kinking. Although deviations from a uniform vertical growth are typically considered to be undesirable, kinking opens a route for additional tweaking of the characteristics and functionalities of NWs in a controllable manner, thus extending the range of potential applications. In the present Review, we give an insight into the kinking mechanisms and summarize the most crucial factors that can lead to kinking of NWs during synthesis. Additionally, the properties and applications of kinked NWs are discussed.

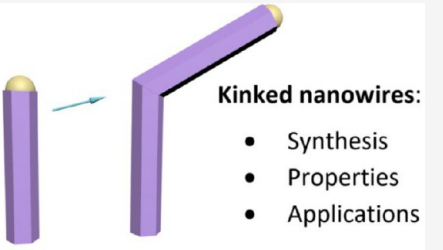

INTRODUCTION

Nanowires (NWs) are solid one-dimensional (high-aspect-ratio) nanostructures that are among the most studied objects in modern material science.[1] Having a diameter in nanometers, NWs exhibit a wide range of unique characteristics, typically attributed to nanoscale objects in general. For instance, they have greatly enhanced mechanical strength,[2,3] increased chemical activity,[4] and other features generally related to quantum confinement and increased surface-to-volume ratio. At the same time, the length of NWs often lies in the micrometric range and can reach tens or even hundreds of μm, allowing for a relatively simple manipulation of individual NWs that facilitates their characterization (e.g., mechanical,[5,6] tribological,[2,7] or electrical[8,9] testing) and the assembly of single-NW-based prototype devices.[10,11] Attractive properties of NWs have inspired a great number of applied studies, in which NWs are tested as key elements of bio/chemical sensors,[12,13] energy-efficient light-emitting devices,[8,14] solar cells,[15,16] photodetectors,[10,17] material for batteries,[18] logic gates,[19,20] field-effect transistors,[8,21] and other nanoelectronic devices.[8]

In order to meet the specific requirements of various applications, it is important to have the ability to tune the properties of NWs by controlling their composition,[3] diameter,[22,23] crystallographic orientation,[24] as well as their defect structure.[25] Usually, defects are intuitively associated with negative effects on the properties of a material. Indeed, defects often cause reduced efficiency, malfunctions, or even failures in various systems.[26,27] However, in spite of a negative flavor in the term, defects can be highly desirable and are widely used to tune the properties of NWs and supplement them with essential functionalities required in particular applications.[28,29] Defects can be created either at the synthesis stage[30,31] or introduced later by post-treatment with plasma,[32,33] chemicals,[34,35] mechanical stresses,[36] etc.

In this work, we focus on a particular type of defect—so-called kinks, i.e., sudden changes in the axial growth orientation of an NW.[37] Similar to other defects, kinks can significantly worsen essential properties of NWs.[38−40] Therefore, in most applications, straight and defect-free NWs are desirable. On the other hand, kinking opens a route for additional control of the characteristics of NWs. Moreover, kinking may give a NW totally new functionalities. In recent years, there is an increasingly growing interest toward kinked NWs because of their potential use in integrated electronic devices, nanoscale springs, nanoelectronic bioprobes, etc.[41−46] Kinking is often reported for semiconductor NWs made of materials having practical significance such as Si,[47,48] Ge,[49,50] GaAs,[51] GaSe,[52] and numbers of other materials. Kinked Si NWs are the most studied ones, having the highest potential to serve as building blocks in electronic[41,53] or nanomechanical devices.[54,55] Moreover, kinks in heterostructures formed by at least two different materials are also reported.[56−58]

Changes in the growth direction are often accompanied by changes in the properties of an NW.[59] Therefore, it is important to understand the mechanisms responsible for these changes. A better control over the kink location and growth direction will allow for advanced spatial NW structures.[42] In the present work, we analyze the available literature dedicated to the kinking of NWs in order to summarize the main methods that allow the controlled introduction of kinks to NWs during synthesis and discuss the impact of the kinks upon properties and behavior of NWs.

Received: July 14, 2021
Published: December 3, 2021

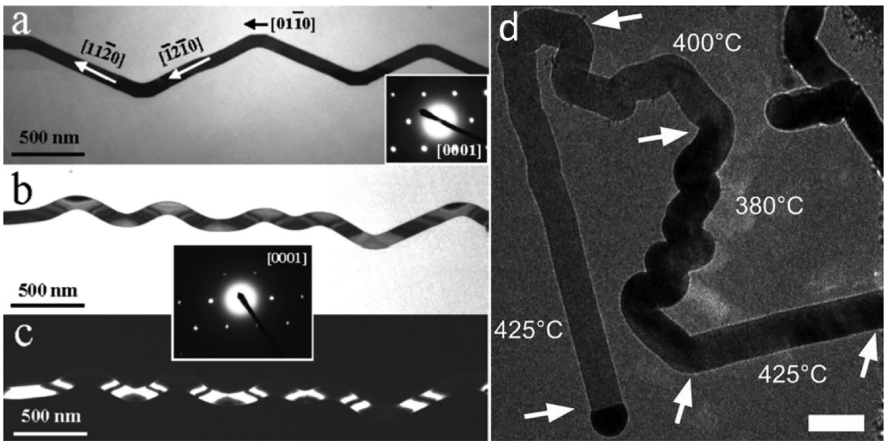

Figure 1. (a,b) Bright-field TEM images and corresponding electron diffraction patterns for zigzag ZnO nanostructures. (c) Dark-field image showing periodic strain inside a zigzag ZnO nanobelt. Adapted from ref 78. Copyright 2004 American Chemical Society. (d) TEM image of a Si NW grown using 2.5 mTorr disilane acquired along the [110] azimuth. Arrows indicate segments grown at different temperatures. The scale bar is 250 nm. Adapted from ref 64. Copyright 2009 American Chemical Society.

KINKING IN NANOWIRES: GENERAL INFORMATION AND KINKING MECHANISMS

Most often, kinking is observed during the synthesis of NWs by any method that involves one-dimensional growth using metal catalyst nanoparticles (chemical vapor deposition, laser ablation, molecular beam epitaxy, etc.). In these types of methods, gaseous precursors are introduced into the reactor either in molecular or atomic form and are gathered and decomposed (for a molecular precursor) on metal nanoparticles. Upon supersaturation of the catalyst particles, the precursor components start to form a crystal seed in the substrate−nanoparticle interface. Continuous supply of precursor components from the gas phase to the solid crystal that grow beneath the particles leads to the formation of NWs with diameters defined by the size of the catalyst. Depending on whether the catalyst is in the liquid or solid state, the growth will follow either the so-called vapor−liquid−solid (VLS)[37,48,60,61] or vapor−solid−solid (VSS)[60−62] mechanisms. The growth direction of NWs is closely related to the surface free energy,[51] since NWs preferentially grow in the direction that minimizes it. The growth direction can change during the synthesis due to changes in some of the key parameters in the system, such as pressure,[42,43,45,47,48,63−65] temperature,[49,50,52,56,64] process time or rate,[41,45,52,63] chemical composition of the atmosphere in the reactor,[41] etc. Although even the simple interruption of the growth process can lead to kinking,[41] typically a change in several parameters is needed. Kinks may appear also as a result of stochastic processes related to the interplay between the surface energies of the NW facets and the interface energy between the catalyst and NW.[37,58,61,62] Often, a mixture of straight and kinked NWs appears in the same sample.[51]

Depending on conditions, the whole kinked NW may have the same crystallographic orientation,[41,66] or kinking can involve a change in crystallographic orientation.[67] In the latter case, kinking occurs mostly between growth directions that are common for the 1D forms of a given material.[60] For instance, the main growth directions for Si NWs are ⟨100⟩, ⟨110⟩, ⟨111⟩, ⟨112⟩, and ⟨113⟩, depending on various factors.[68] For the most widespread Au-catalyzed VLS growth, ⟨111⟩ growth is observed for diameters >40 nm, ⟨110⟩ for diameters below ∼10 nm, and a mixture of ⟨112⟩ and ⟨111⟩ for diameters ranging from ∼10 to 40 nm. This is valid for both epitaxially[68] or nonepitaxially[69] grown Si NWs. VSS-grown Cu-catalyzed Si NWs favor the ⟨110⟩ direction, with occasional growth along ⟨111⟩.[70] Al-catalyzed Si NWs grow epitaxially along ⟨111⟩, normal to the {111} Si substrate surface;[71,72] ⟨110⟩ Al-catalyzed Si NWs can grow epitaxially on {110}-oriented Si substrates.[73] For Ga-catalyzed VLS growth,[74] all ⟨110⟩, ⟨112⟩, ⟨111⟩, and ⟨100⟩ growth directions have been reported.[75] For In-catalyzed growth, the variety of Si NWs growth directions include ⟨100⟩, ⟨111⟩, ⟨112⟩, and ⟨113⟩, depending on the NW diameter.[76] When there are multiple growth directions that are nearly equally favorable, small changes in the growth conditions can shift the balance between them.[77,78]

NWs can have single[56,79] or multiple kinks (multikinked NWs).[79] In the latter case, periodically modulated structures sometimes referred to as zigzag[52,78,80] (Figure 1a−c), sawtooth,[81,82] or even wormy[64] (Figure 1d) NWs may appear. The mechanisms responsible for periodic kinking may vary for different materials and conditions. For instance, anisotropic sawtooth structures observed for wurtzite ZnO, ZnS, and CdSe were explained by the equilibrium crystal surface structure.[81] The formation of sawtooth-type Si NWs in the VLS process was linked to a periodic shrinking and expansion of the liquid catalyst, induced by the interplay between surface energy and geometry of NWs and the catalyst droplet.[52] Sawtooth and zigzag morphologies in GaSe NWs supposedly related to the participation of Ga in the catalyst.[52] A liquid Ga catalyst droplet has a lower surface-interfacial energy compared to Au, and its shape is more sensitive to perturbations during growth, which results in a constant change in growth direction that leads to formation of zigzag and sawtooth structures. The authors of ref 52 conclude that liquid droplets are perturbed by the combination of surface-interfacial energy, thermal energy, gas flow, or other mechanical motions.

Kinking often involves dropping of or displacing the metal catalyst.[59,61,83] As observed by Dick et al.[57] for heterostructured NWs, once the nucleus of a new material is formed on the already grown part decorated with the catalyst, further growth can displace the catalyst asymmetrically. Thus, the NW gets kinked or even folds over to grow backward (Figure 2). Furthermore, Sivaram et al.[84] attributed the appearance of kinked Ge NWs to the rapid expulsion of Ge atoms from the solid AuGe catalyst, as has been also observed previously.[85]

https://doi.org/10.1021/acs.cgd.1c00802
Cryst. Growth Des. 2022, 22, 871−892

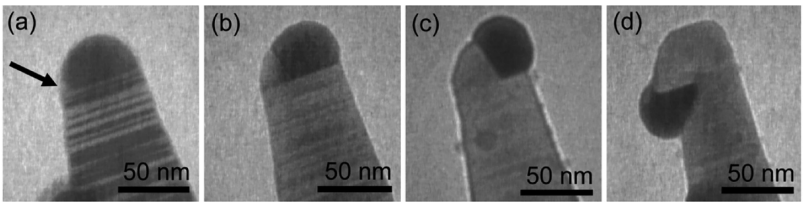

Figure 2. Bright-field TEM images recorded during the growth of Ge on GaP NWs by UHV−CVD. Images represent different wires. (a) After the Au particle becomes saturated with Ge, nucleation is observed as a small compact Ge crystal at the boundary between GaP, Au, and the vacuum. This brighter nucleus is indicated by an arrow. The horizontal lines are stacking faults. (b) As the nucleus enlarges, the Au particle is pushed horizontally across the GaP surface. Ge does not form a layer on the GaP. (c) As the growth proceeds, a new growth front is visible between the Ge and Au, apparently a different (111) interface. (d) When the particle reaches the edge of the GaP, the growth may continue outward from the wire or may wrap around the top. Adapted from ref 57. Copyright 2007 American Chemical Society.

Kinks are often accompanied by crystallographic defects such as twin boundaries. Characteristic examples are the kinking of non-centrosymmetric crystalline NWs during their growth along the polar axis[66] and the kinking of Si NWs that involves segments of ⟨112⟩ axial orientation.[83,86] He et al.[60] demonstrated that most turning angles in kinked Si NWs can be considered as various combinations of different types of {111} coherent twins that coexist at the transition regions between different segments. Thicker NWs have a higher concentration of defects, leading to situations where a mixture of thin straight and thick kinked NWs is obtained from the same material during a synthesis.[62] For instance, inclined defects may affect the geometry of NW,[58] making the change in growth direction easier. There is also a so-called coherent kinking that does not have defects around the kink.[37,58,64] For example, coherent kinking is observed in Ge NWs for diameters at which ⟨111⟩ and ⟨110⟩ VLS growth orientations are almost equally favored, governed by the balance of surface/interface energies.[66,87,88] Coherent kinking from the vertical [111] orientation to an inclined ⟨111⟩ axis can be caused by an error in the sidewall facet development as the cross section area of the NWs is rapidly reduced, while the catalyst droplet "lifts off" the substrate surface.[88,89]

Surface adsorbates can alter the NW sidewall energies and promote kinking, as has been observed for the Au sidewall wetting during VLS growth of Si NWs.[64] According to Filler et al.,[67] kinking of Si NWs and subeutectic VLS growth of Ge NWs[84] (using a Au catalyst in both cases) is strongly influenced by hydrogen adsorption on the sidewalls of NWs.

Generally, kinking in the VLS process is closely related to the stability of the triple boundary between the liquid catalyst droplet, the solid NW, and the gas phase.[57] In the dynamic model of the VLS process developed by Schwarz and Tersoff,[90,91] the growth is controlled by the balance of capillary forces acting on the triple boundary line, combined with the difference in chemical potential between the liquid and solid phases. They propose that many of the complex morphological phenomena observed during NW growth can be explained by the interplay of only three elementary processes: facet growth, droplet statics, and the introduction of new facets. Their model agrees well with most of the experimental data related to NWs and kinking.

Although kinking is observed mostly in VLS and VSS processes, kinks can occur also during catalyst-free NW synthesis. For instance, Geaney et al.[49] observed kinking in Ge NWs synthesized via the catalyst-free metal−organic vapor-phase route. The authors attributed these kinks to the interplay between the NW's tendency to grow along a preferred crystallographic axis and defects perpendicular to the growth direction. These catalyst-free (seedless) synthesis processes are less understood and have been utilized less frequently than seeded methods so far. Moreover, sometimes fundamentally different approaches are used, such as anisotropic etching of the substrate.[92] A more detailed description will be given in the next section.

SYNTHESIS OF KINKED NWS: CRITICAL PARAMETERS

There are several different strategies used to obtain kinks in NWs. The most common approaches rely on changing certain parameters during the synthesis—mainly temperature and pressure. Modulations in precursor composition or molar flow rate are also used rather often. Other methods are based on tweaking some characteristics prior to synthesis (e.g., catalyst particle size, choice of substrate). It should be also noted that the growth parameters are not necessarily independent of each other and modification of one may influence the other. In this section, we briefly overview chosen works that involve synthesis of kinked NWs in order to highlight the most common factors and quantitative parameters responsible for kinking during growth.

Temperature. The growth direction of NWs is known to depend on the temperature in the reactor.[42] If the temperature is varied during the synthesis, it may result in a change of the growth direction of an already growing NW. Therefore, it is fair to say that the temperature is probably the simplest and most straightforward parameter that can be tweaked in order to achieve or avoid kinking. However, the mechanisms responsible for kinking at certain temperatures may be not that obvious. Two distinct scenarios have been reported in the literature: depending on the system and method, kinking may happen either at "lower-than-optimal" or "higher-than-optimal" growth temperatures. To understand the role of temperature in the formation of kinks, it is important to briefly discuss a few thermal aspects of the VLS growth of NWs in general. According to the logic that is reflected in the name of the VLS mechanism, NWs are expected to grow by the incorporation of material from the vapor into the growing NW via a liquid catalyst, commonly a low-melting-point eutectic alloy. However, the growth of NWs at temperatures below the eutectic temperature with either liquid or solid catalysts at the same temperature has often been observed.[85] The catalyst state was shown to be dependent on the growth pressure and thermal history, which has been explained by the kinetic enrichment of the eutectic alloy composition.[85] At temperatures "lower-than-optimal", NW growth becomes unstable and prone to kinking, as the process is not perfectly epitaxial.[93,94]

A good example of subeutectic growth is given in the study performed by Kim et al.,[50] where the authors exploited the

https://doi.org/10.1021/acs.cgd.1c00802
Cryst. Growth Des. 2022, 22, 871−892

growth of Ge NWs on Si (111) substrates by CVD with Au nanoparticle catalysts at different temperatures (Figure 3). They found that for temperatures above 270 °C, the grown NWs are straight and vertically aligned (Figure 3a–d). When the temperature is decreased to 260 °C, the NWs start to kink (Figure 3e), while the growth is terminated at temperatures below 250 °C (Figure 3f). The authors suggest that such an abrupt change in the NW morphology indicates that a rapid solidification of the catalyst occurs at 260–250 °C, because the liquid phase cannot be maintained at such a low temperature. This indicates that kinking is achieved only within a very narrow temperature range, in which the transition between the solid and liquid state of the catalyst is expected. Multiple kinks and tortuous morphology were reported[62] for ⟨111⟩-oriented Ge NWs, synthesized by low-temperature (in the range of 300 to 375 °C, below the eutectic reaction in the Ni–Ge system) VSS growth, using a NiGe catalyst. In another work by Kim et al.,[86] kinked Ge NWs have been successfully formed on a Si substrate at subeutectic temperatures by a purging/nucleation process. The nucleation was performed at 350 °C for 2 min followed by NW growth for 20 min at a subeutectic temperature of 300 °C. Multiply kinked NWs were grown, and the segment length was controlled by growth time. According to the authors, the Au catalysts were in the liquid state at the subeutectic temperature, and thereby, the growth of Ge NWs still proceeds under the VLS mechanism. Their finding is in a good agreement with Hillerich et al.[56] who showed that increasing the temperature increases the number of straight NWs.

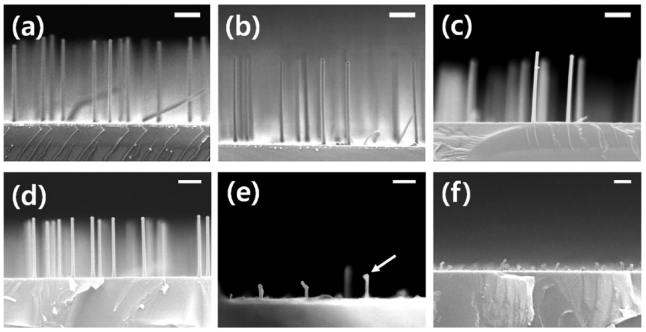

Figure 3. Field emission SEM images of Ge nanowires on GeBSi substrates grown at (a) 300 °C, (b) 290 °C, (c) 280 °C, (d) 270 °C, (e) 260 °C, and (f) 250 °C for 20 min. The arrow points at the kink in the NW. Scale bar = 500 nm. Adapted from ref 50. Copyright 2011 American Chemical Society.

On the other hand, "higher-than-optimal" temperatures may induce a number of deviations from regular growth, including significant radial overgrowth manifested as NW tapering,[95,96] undesirable shell structures,[97] and compositional nonuniformity along the length of ternary NWs.[98] The density of crystallographic defects may also increase with growth temperature.[99] Already back in 1968, Wagner et al.[100] demonstrated that if temperature is abruptly increased, it may induce the displacement of the droplet, leading to the formation of kinks or branches. Since then, kinking as a result of increased temperature has been demonstrated in numerous studies. Li et al.[37] studied the morphologies of kinked Ge NWs synthesized in a cold-wall CVD chamber using Au catalysts and found up to a 6-fold (depending on diameter) increase in the fraction of kinked NWs as the growth temperature increases from 390 to 420 °C. Peng et al.[52] synthesized GaSe NWs using Au-catalyst-assisted VLS at relatively high temperatures (800–900°). For both synthesis temperatures, the authors found multiply kinked zigzag and sawtooth NWs, with kinking angles that were uniformly 120°. However, the relative yield of kinked NWs was significantly higher at higher temperatures. Song et al.[101] observed kinking near the base of epitaxial Ge NWs grown by CVD at any temperature in the range required for synthesis (from 300 to 380 °C). However, the kinking was more prominent for NWs grown at higher temperatures. Geaney et al.[49] also observed a significant increase in the relative proportion of kinked Ge NWs to straight ones, when the temperature of the synthesis was increased. However, it is important to note that they used metal–organic chemical vapor deposition (MOCVD) without a catalyst; therefore, there are no eutectics involved. Moreover, the NWs were periodically twinned, which may be another important factor in relation to kinking. A link between kinks and stacking fault content in the NWs was found. The interplay between the preferable NW growth direction and the defect orientation was found to dictate the morphology of these NWs. Growth-direction-driven large-angle kinks prevailed, while the occurrence of defect-driven small-angle kinks was small.

Finally, we would like to note that the measurement of the growth temperature is often performed indirectly, and the

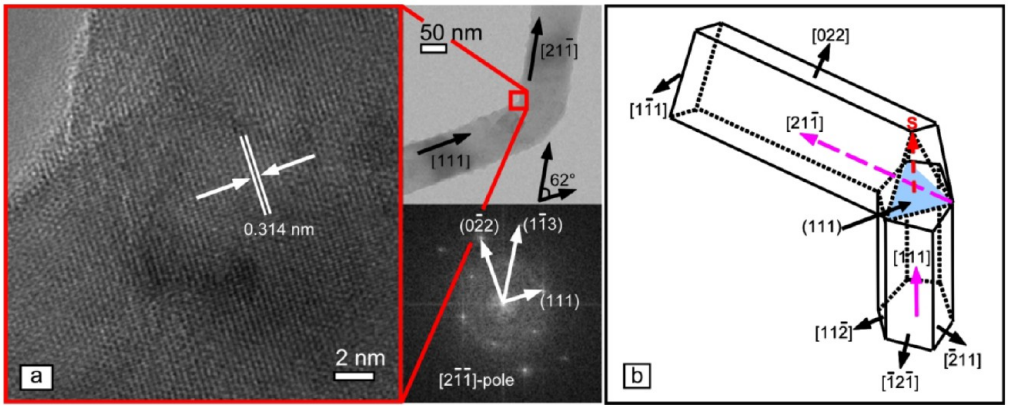

Figure 4. (a) TEM image of a kinked Si NW grown in the two-step process. The (111) lattice planes of a [111] growth direction wire have grown continuously within the [21$\bar{1}$] wire. (b) Schematics of the crystallographic relationship between growth directions of a kinked Si NW. Reprinted with permission from ref 48. Copyright 2009 IOP Publishing.

https://doi.org/10.1021/acs.cgd.1c00802
Cryst. Growth Des. 2022, 22, 871–892

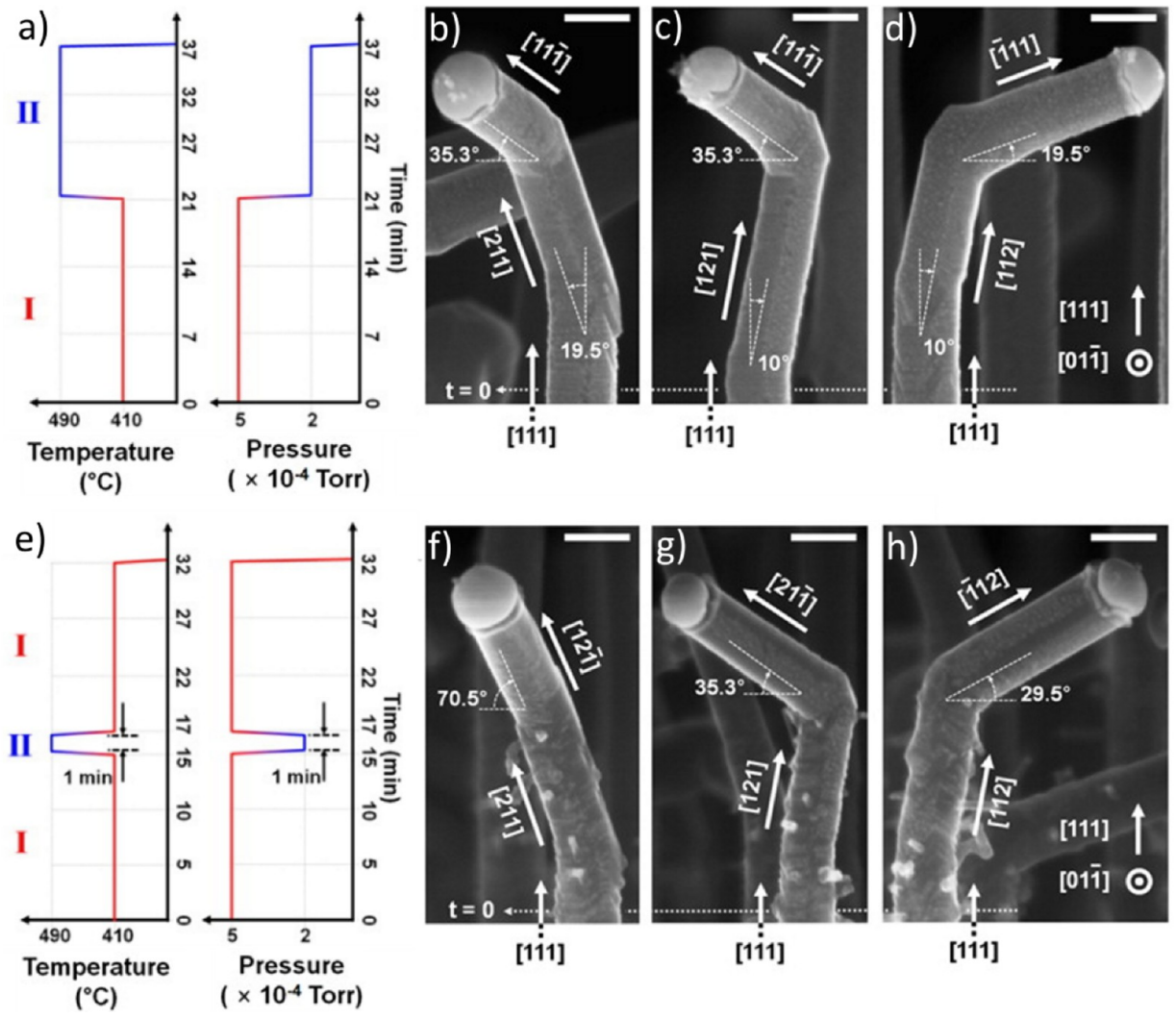

Figure 5. (a) Substrate temperature and disilane pressure as a function of time for ⟨211⟩ → ⟨111⟩ kinking for conditions I and II. SEM images along the [01$\bar{1}$] direction of Si NWs showing a ⟨211⟩ → ⟨111⟩ kinking: (b) [211] → [11$\bar{1}$], (c) [121] → [11$\bar{1}$], and (d) [112] → [$\bar{1}$11]. (e) Substrate temperature and disilane pressure as a function of time for ⟨211⟩ → ⟨211⟩ kinking. SEM images along the [0$\bar{1}$1] direction of Si NWs showing ⟨211⟩ → ⟨211⟩ kinking: (f) [211] → [12$\bar{1}$], (g) [121] → [21$\bar{1}$], and (h) [112] → [$\bar{1}$12]. Both types of kinked NWs have [111] segments at the base and are grown for 10 min under condition II. The axial positions where condition I is initially applied are indicated with dotted lines at the lower part of SEM images. Scale bars are 100 nm. Adapted from ref 67. Copyright 2014 American Chemical Society.

approach may vary across different growth systems. These aspect should be taken into account when interpreting and comparing results from the research community.

Pressure. Pressure (both total pressure[47,48] and precursor partial pressure[73]) is another common factor that influences the growth direction of NWs and is often varied during the synthesis in order to introduce kinks.

Already in relatively early studies dedicated to the synthesis of Si NWs by the Au-catalyzed VLS process using silane (SiH_4) as the Si source gas, it was shown that decreasing the partial pressure of silane leads to an increase in NW diameter and reduces the amount of growth defects.[93] Later, Lugstein et al.[47] studied the influence of silane pressure on the epitaxial growth of Au-catalyzed Si NWs on Si(111) via a VLS process at 500 °C. They found that at 3 mbar, the NWs grow preferentially in the ⟨111⟩ direction, while at 15 mbar, the ⟨112⟩ direction is favored. When the pressure was abruptly switched during the synthesis, NWs that were already growing kinked and changed their growth direction without changing their diameter. The same year, Schmid et al.[102] also reported a growth direction change for epitaxial Si NWs grown on Si (111) substrates by CVD when they kept total reactor pressure constant but varied the partial pressure of silane. Shortly afterward, their results were confirmed with the same material and conditions by Hyun et al.[48] Pressure-controlled kinking between the [111] and [211] growth directions was obtained with an angle between straight segments of 62° (Figure 4). These results clearly demonstrate that kinking in Si NWs can be introduced in a well-controllable manner.

Schmid et al.[102] also studied kinking in silicon NWs grown by VLS on Si(111), using an Au catalyst and silane as a precursor. They performed two sets of experiments. In the first set, the SiH_4 partial pressure was varied between 50 and 400 mTorr while keeping the temperature constant. In the second set, the temperature was varied from 470 to 600 °C at constant pressure of 80 mTorr. For the first set, it was found that at lower pressure the preferred growth direction is vertical.[111] At higher partial pressures, increasingly more NWs kinked to one of the other three possible directions of the ⟨111⟩ family. For the second set, kinking increased significantly with temperature.

https://doi.org/10.1021/acs.cgd.1c00802
Cryst. Growth Des. 2022, 22, 871−892

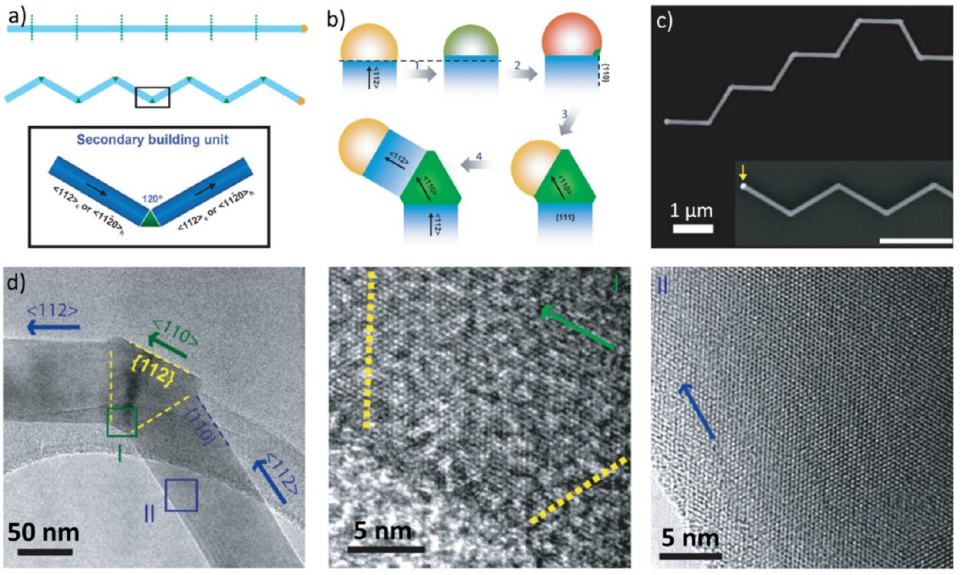

Figure 6. (a) Schematic of a coherently kinked NW and SBU containing two arms (blue) and one joint (green). The multiply kinked NWs (middle panel) are derived from the corresponding 1D NW by introducing the joints at the locations indicated by the dashed lines in the upper panel. Subscripts c and h denote cubic and hexagonal structures, respectively. (b) Schematic illustrating the key stages of kink formation. Arrows 1−4 denote purge, reintroduction of reactant, joint growth, and subsequent arm growth, respectively. (c) SEM images of the kinked Si NW (upper) grown with periodic 15 s purges. Inset: SEM image of a multiply kinked 2D silicon NW with equal arm segment lengths. The arrow indicates the location of the catalyst. (d) TEM image of a single kink with crystallographic directions and facets indicated by arrows and dashed lines, respectively. The green (I) and blue (II) squares correspond to high-resolution images in the two last panels. Dashed lines and solid arrows indicate crystallographic planes and growth directions, respectively. Reprinted with permission from ref 41. Copyright 2009 Springer.

Another study dedicated to kinking of Si NWs grown from Au seeds on a Si(111) substrate was performed in the same period by Madras et al.[64] However, as compared to the above-mentioned studies, here the authors used disilane instead of silane. In addition to varying the pressure, the influence of the temperature on the growth process was also exploited. They found that Si NWs growing perpendicularly to the substrate can be induced to kink away from [111] by either reducing the substrate temperature (from 500 to 400 °C) or increasing the disilane pressure (from 0.2 to 10 mTorr). An important finding was also that for growth at 400 and 500 °C, the NWs kinked mostly toward another ⟨111⟩ direction at lower disilane pressures and preferred the ⟨112⟩ direction at higher disilane pressures. The authors explained this observation to the inability of Au to wet the NW sidewalls at the higher silane pressure, causing the initially [111]-oriented NWs to switch to a lower-energy ⟨112⟩ growth axis, which agrees with the results reported in ref 47.

Later, Shin and Filler[103] studied kinking of Si NWs in a silane atmosphere further at different pressures and temperatures. They found that the hydrogen originating from the Si_2H_6 precursor is responsible for kinking. The authors continued their study,[67] revealing the interplay between growth orientation, defect propagation, and surface chemistry. In the latter work, kinking was obtained by switching between two growth conditions that involve changes both in pressure and temperature:

(1) Condition I: 5×10^{-4} Torr Si_2H_6 and 410 °C.

(2) Condition II: 2×10^{-4} Torr Si_2H_6 and 490 °C.

The authors observed multiple degenerate kink directions as shown in Figure 5.

A more recent study on the kinking of Si NWs grown in silane atmosphere was conducted by Hainey et al.[73] This time, Al catalysis was used instead of the more traditional Au, and the NWs grew in the ⟨110⟩ and ⟨111⟩ directions. The authors tested the effect of hydrogen partial pressure by varying the reactor pressure from 100 to 500 Torr in 100 Torr increments. At 100 Torr, NW growth was nonepitaxial, resulting in all or at least most of the NWs being extensively kinked. This may be due to the vapor−solid deposition of amorphous silicon on the tip and sidewalls of the NWs during synthesis. The amorphous coating may destabilize the Al catalyst/NW interface during the growth, promoting the kinking. Kinking was observed for the majority of NWs also at 200 Torr, especially at the tips of the wires. This was explained by catalyst destabilization occurring at lower pressures. With increasing the pressure to 300 Torr, significant kinking was still observed, but the yield of vertical wires increased further. However, starting from 300 Torr and above (up to 500 Torr), the amount of kinking did not significantly change further, suggesting that this pressure is sufficient for suppressing the rate of vapor−solid deposition of silicon.

Multiple-pressure modulation was recently described by Sun et al.,[65] for Au-catalyzed Si NWs grown in a hot-wall CVD reactor at 450 °C and a total pressure of 40 Torr using a silane precursor, H_2 as a carrier gas, and B_2H_6 (100 ppm in He) as the doping precursor. Kinking was introduced by temporally decreasing the pressure to 3.5 Torr for 10 s followed by restoration of initial value. Pressure modulations was repeated every 2−4 min for a total of 10 cycles. The resulting kinking probability was approximately 50% for a 100 nm diameter ⟨211⟩ NW.

Xu et al.[45] demonstrated an exceptional degree of control in the formation of U-, V-, and W-shaped kinked Si NWs in Au-catalyzed VLS growth. NWs were grown at 40 Torr and 460 °C. To introduce one 120° kink, the growth was paused for 15 s to introduce kinks by rapidly evacuating the chamber to the lowest pressure and shutting down the gas lines. The procedure was

https://doi.org/10.1021/acs.cgd.1c00802
Cryst. Growth Des. 2022, 22, 871−892

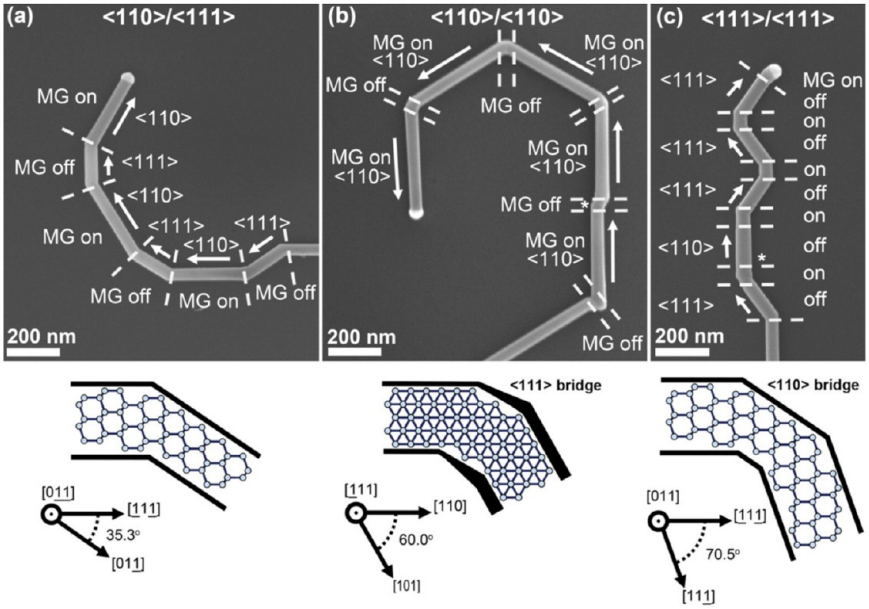

Figure 7. SEM images of (a) ⟨111⟩/⟨110⟩, (b) ⟨110⟩/⟨110⟩, and (c) ⟨111⟩/⟨111⟩ Ge NW superstructures grown at 325 °C by introducing and removing MG during synthesis. An asterisk indicates the locations where transition did not occur as planned. Schematics for each growth direction change are shown below each corresponding superstructure with the smallest deviation angle labeled. Bolded sidewalls in the schematic for (b) denote that the diamond cubic lattice dictates that neighboring ⟨110⟩ segments of the ⟨110⟩/⟨110⟩ superstructure cannot lie in the same plane. Adapted from ref 104. Copyright 2012 American Chemical Society.

repeated for a sufficient amount of times to obtain the required geometries.

It should be noted that although a modulation of global process parameters such as precursor partial pressure or substrate temperature is a simple way to achieve kinking, multiple aspects of NW morphology (surface defects, tapering, etc.) can be undesirably impacted by this approach.[104−108] Therefore, alternative methods are constantly being developed and are actively studied as will be shown further in this Review.

Vapor/Gas Composition. The composition of the atmosphere in the reactor during a VLS growth process can be modulated in order to achieve certain morphologies and more complex compositions such as heterostructured NWs. This can also lead to kinking as a result of changes in vapor or gas composition, especially when the precursor is modulated. Moreover, the location of the kink introduced by this method can be controlled with high accuracy.

Schwarz et al.[77] reversibly switched the orientation of Au-catalyzed Si NWs during *in situ* TEM growth by introducing or ceasing a small flow of O_2, adapting a method published earlier.[109] According to the authors, oxygen changes the relative energies of {111} and {113} facets so that either one or the other growth direction is favored. Joyce et al.[110] reported a transition from vertical to kinked GaAs NWs by increasing the ratio of arsenic (group V) to trimethylgallium (group III precursors) in Au-catalyzed metal−organic CVD synthesis.

Tian et al.[41] utilized the so-called "nanotectonic" approach for synthesis of two-dimensional kinked Si NW chains using the Au-catalyzed VLS process. The idea behind nanotectonics is the spontaneous or directed assembly of nanoscale building blocks into organized structures.[111] Similarly to metal−organic framework materials, the authors created a secondary building unit (SBU) consisting of two straight single-crystalline arms connected by one fixed 120° angle joint (Figure 6a). SBU formation procedure includes three main stages:

(1) Axial growth of a straight NW arm segment.
(2) Purging of gaseous reactants to suspend NW growth and induce perturbation.
(3) Supersaturation and initiation of NW growth following reintroduction of reactants.

The concentration of the silicon reactant dissolved in the nanocatalyst drops during purging and then reaches a maximum upon supersaturation.

The kink formation is shown schematically in Figure 6b. Arrows 1−4 indicate purge, reintroduction of reactant, joint growth, and subsequent arm growth, respectively.

SEM images of kinked silicon NW with a 150 nm diameter, (upper) grown with periodic 15 s purges, are shown in Figure 6b. The inset shows an SEM image of a multiply kinked 2D silicon NW with equal arm segment lengths. The arrow indicates the position of the nanocatalyst. TEM images of a single kink (Figure 6d) revealed no twin defects or stacking faults, confirming that the entire arm−joint−arm junction has a single-crystal structure. Steps (1) to (3) can be repeated to bond a number of SBUs, resulting in a two-dimensional chain structure.

Musin and Filler[104] demonstrated that the introduction of a methylgermane ((GeH_3CH_3), MG) to a growth environment of Ge NWs (GeH_4/H_2) can change the growth direction and lead to kinked superstructures with controllable segment lengths and angles. Ge NWs grown using only the traditional GeH_4/H_2 chemistry always yield a ⟨111⟩ orientation. The growth, however, can be temporarily switched to ⟨110⟩ and then back to ⟨111⟩ if MG is introduced and removed from the growth environment at temperatures below 425 °C. Authors repeated the procedure multiple times obtaining complex multikinked structures. Examples of ⟨111⟩/⟨110⟩, ⟨110⟩/⟨110⟩, and ⟨111⟩/⟨111⟩ superstructures grown at 325 °C with a corresponding schematic of each kink type is shown in Figure 7. Kinked NWs remained single-crystalline, and no twin defects or stacking faults

https://doi.org/10.1021/acs.cgd.1c00802
Cryst. Growth Des. 2022, 22, 871−892

were observed near the kink. MG also created a passivating layer on the sidewalls of NWs, preventing tapering and significantly expanding the process window for Ge NW growth from hydride-based precursors. At temperatures above 475 °C, no deviation from ⟨111⟩ growth was observed even in the presence of MG.

Wang et al.[112] demonstrated that by changing the catalyst composition and shape *in situ*, it is possible to switch the growth direction of InP NWs between ⟨100⟩ and ⟨111⟩ in the VLS process, in a controllable manner. The process started with the production of vertical ⟨100⟩ InP NW arrays on a Au−In catalyst, under trimethylindium (TMI) and phosphine (PH_3) flow. TMI is important for maintaining the In content in the catalyst droplet and avoiding the destabilization of the droplet's shape. Then, TMI was switched off, while PH_3 flow was kept on. The wires continued to grow while the In fraction in the droplet gradually decreased below the supersaturation level required for NW growth. For In depletion times exceeding 1.5 min, the growth direction of NWs switched from ⟨100⟩ to ⟨111⟩. Switching occurred uniformly across the entire substrate. Next, the authors demonstrated the ability to switch the growth direction back from ⟨111⟩ to ⟨100⟩. After growing in the ⟨100⟩ and ⟨111⟩ directions consecutively, the PH_3 was switched off while TMI was kept on for different periods. As a result, the growth was interrupted, and the In was absorbed by the catalyst droplet from TMI decomposition. Then, the PH_3 was switched back on before cooling down.

Zhang et al.[113] reported a somewhat similar approach to control the growth direction of defect-free zinc blende InAs NWs in molecular beam epitaxy (MBE) by carefully controlling the In content in the Au catalyst. When an In source is introduced to the reactor, In atoms diffuse into the Au catalyst to form Au−In alloy nanoparticles. Au−In particles with lower In content tend to initiate vertical ⟨000$\bar{1}$⟩ NW growth, while a higher indium concentration induces the epitaxial growth of ⟨00$\bar{1}$⟩ NWs.

Shin and Filler[103] controlled the growth direction of VLS-grown Si NWs via surface chemistry. Kinking was achieved upon the addition of hydrogen on the NW's sidewall. The authors demonstrated that covalently bonded hydrogen atoms are responsible for the commonly observed growth transition in Si NWs from ⟨111⟩ to ⟨112⟩.

Kinking can be achieved also when different segments of an NW have different chemical composition. For instance, Dick et al.[57] studied the growth of various heterostructured NWs (combinations of the III−V materials GaAs, GaP, InAs, InP, AlAs, as well as Si) by changing the precursor composition during synthesis by Au-catalyzed low-pressure metal−organic vapor-phase epitaxy (LP-MOVPE). No annealing was performed between the synthesis of segments with different composition. The hydrogen was used to flush the reactor between growth of the two different compositions to remove precursor residuals. The authors highlighted two typical growth categories. In some systems (GaP on InP or GaP on Si), the NW growth continued in the same crystal direction after introduction of the second material (Figure 8a). In other cases (InP on GaP, Si on GaP, InAs on GaAs, InAs on AlAs), NWs kinked (Figure 8b) or even wrapped around themselves and grew backward (Figure 8c). Note that the same pair of materials may or may not produce kinked nanostructures, depending on which material was grown first (e.g., GaP/Si). In general, the authors did not observe a mixture of straight and kinked morphologies—mostly either only straight or only kinked morphologies (often approaching 100%)—were observed for a given material combination for all growth conditions. Dick et al., as well as Ross et al.,[43] speculated that for heterostructured NWs that do not kink, the second material grows in a layer-by-layer mode, while for the ones that do kink, the second material grows from a compact nucleus.

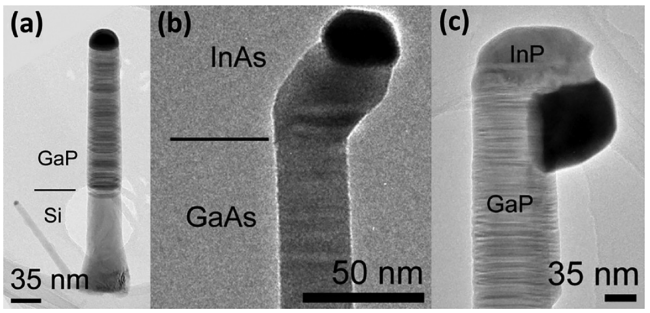

Figure 8. TEM images of heterostructured kinked NWs. (a) Si → GaP NW. The Si part is single-crystalline, while the GaP part exhibits extensive stacking faults perpendicular to the growth direction. (b) GaAs → InAs NW. The interface between materials is indicated by a line. (c) GaP → InP NW. The InP wraps along the top of the GaP and grows backward. Adapted from ref 57. Copyright 2007 American Chemical Society.

A drastic change in the growth direction of heterostructured NWs was observed also by Paladugu et al.,[59] for InAs segments grown on GaAs NWs. InAs/GaAs heterostructures were grown using Au nanoparticles of ∼30 nm diameter as catalysts, in a horizontal-flow metal−organic chemical vapor deposition (MOCVD) reactor. The growth pressure and temperature were 100 mbar and 450 °C, respectively. GaAs NWs were grown on a {111}B GaAs substrate by flowing trimethylgallium (TMG) and AsH_3 into the chamber. Then, InAs NW sections were grown on the GaAs NWs by replacing the TMG flow with a TMI while maintaining the AsH_3 flow. It was found that thinner NWs tend to bend more than thicker ones. SEM and TEM studies revealed that in the case of thinner NWs, the Au particle has moved away from the tip region down the NW, while for the thicker ones, a sideward movement of the Au particle was observed (similar to the process of Figure 2). Since during GaAs growth the Au particles remained on top of the NWs,[98] these Au movements must take place during the InAs growth period. In their work, the authors provide an in-depth analysis of the mechanisms responsible of the observed behavior and results. Shortly, they conclude[59] that the axial growth failure of InAs on GaAs NWs is explained by the lower Au/GaAs interfacial energy as compared to Au/InAs. In general, when an axial NW heterostructure is grown by the VLS mechanism with two materials A and B, through a catalyst particle C, if the interfacial energy between A and C is higher than that between B and C, the axial growth of A on B fails, whereas the axial growth of B on A is feasible.

Svensson et al.[63] studied the kink formation in InAs−InP heterostructured NWs grown by chemical beam epitaxy (CBE) on InAs (111)B substrates, using TMI, tertiarybutylarsine (TBAs), and tertiarybutylphosphine (TBP) as precursors. The authors studied the impact of different parameters (pressure, NW density and diameter) on the probability of kinking and found it to be always dependent on the amount of available In in the system. Kinking always occurred at the InP → InAs interface. By tweaking the growth parameters, the authors were able to increase the yield of kinked NWs up to 68%.

https://doi.org/10.1021/acs.cgd.1c00802
Cryst. Growth Des. 2022, 22, 871−892

Kinking in hybrid NWs was observed also by Dayeh et al.[58] for VLS-grown Au-catalyzed Ge−Si NWs. The authors utilized precise sequencing of the gas precursor partial pressure and temperature upon transitioning from Ge to Si during growth. This resulted in pure Ge and pure Si NW segments with dimensions suitable for a detailed structural study and potential applications. A 19.5° change in growth direction was observed between segments at certain growth rates, which was attributed to the formation of twin boundaries. Ref 58 contains a detailed high-resolution structural analysis and atomistic modeling of the nucleation and propagation of stacking defects throughout single NWs, greatly contributing to the understanding of the NW kinking mechanisms.

Size Factor (Catalyst Manipulation). In numerous studies, a clear connection between the diameters of the NWs and the probability of kinking was observed. Considering that the NW diameters in both the VLS and VSS processes are directly related to the size of the catalyst particles, the proper choice of the catalyst particle size is another factor that can be used to manipulate the amount of kinked NWs in a sample.

Thombare et al.[62] reported a strong dependence of the morphology on diameter of Ge NWs synthesized by low-temperature VSS growth using a NiGe catalyst. NWs with diameter below 25 nm were straight and grew preferentially in the ⟨110⟩ direction. NWs with diameter exceeding 25 nm were ⟨111⟩-oriented, had a high density of defects, and exhibited multiple-kinking, resulting in a tortuous shape. The authors demonstrated that kinking in thicker NWs involves multiple twinning events facilitated by the slow growth and anisotropic catalyst/wire interfaces, typical for VSS growth. Such effects are expected also for other VSS systems where the NWs exhibit different morphologies. According to TEM observations, NWs with a tortuous morphology had catalyst particles larger than 25 nm, while particles on straight NWs were smaller than 25 nm. This clearly indicates that the diameter of catalyst particles is the deciding factor that can be chosen correspondingly to either induce or avoid kinking.

Hillerich et al.[56] introduced conditions that decreased the Au droplet volume during the growth of a pure Si NW in the UHV TEM at 645 °C in 1.1×10^{-6} Torr disilane. Gold is highly mobile on the silicon surface, and its migration leads to Ostwald ripening: Au atoms detach from a droplet, diffuse across the surface, and rejoin the same or another droplet. As the droplets shrink, the corresponding NW diameters also decrease, and inclined sidewall facets are formed. This sequence of events results in a single kink without other defects. The authors speculated that if a droplet is "too small" for the initial area, it grows a segment that decreases in diameter resulting in inclined (111) sidewall facets. The droplet then moves to an inclined facet, and growth continues in a kinked ⟨111⟩ direction. Once kinked, the new diameter is correctly matched to the droplet volume and contact angle, and no further kinking is required. This scenario is summarized in Figure 9.

Madras et al.[64] studied Au-catalyzed Si NWs, grown in a disilane atmosphere. They found that the probability of kinking depends on the NW diameter for most experimental conditions (temperature and disilane pressure) except one (500 °C, 0.7 mTorr) as summarized in Figure 10. Moreover, the growth direction after kinking was also found to be dependent on the NW diameter. The smallest ($D < 20$ nm) Si NWs kinked toward ⟨110⟩, while larger ($D > 40$ nm) NWs favor either ⟨111⟩ or ⟨112⟩, depending on whether or not growth conditions favor Au wetting the NW sidewalls.

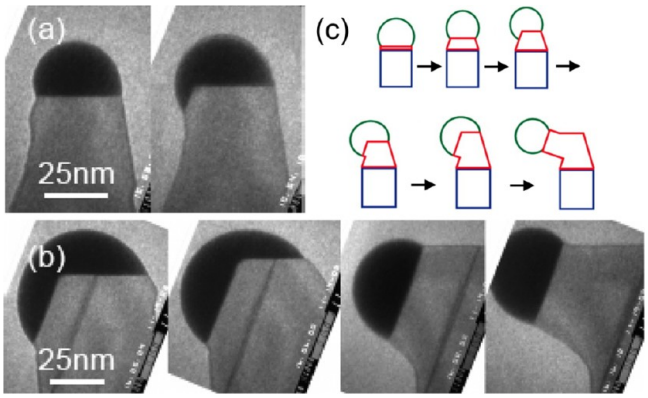

Figure 9. Chosen frames of Si NWs growth inside UHV TEM under conditions of decreasing droplet volume. The electron beam is parallel to ⟨110⟩. (a) Migration of Au from the droplet (Ostwald ripening) reduces the droplet volume. The NW diameter decreases via formation of inclined (111) facets. (b) A different NW with a larger inclined facet. (c) Schematic diagram showing the outcomes for NW morphology in the case of a mismatch between the droplet volume/contact angle and the NW diameter. Adapted from ref 56. Copyright 2013 American Chemical Society.

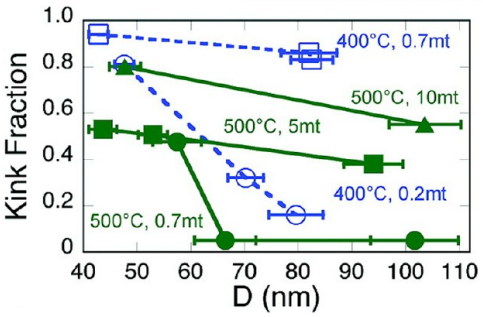

Figure 10. Fraction of NWs that kink away from [111] vs average diameter, D, at the indicated P in mtorr (mt) and T. Adapted from ref 64. Copyright 2009 American Chemical Society.

A dependence of the kinking probability on the catalyst size and corresponding NW diameter was reported also by Li et al.[37] for CVD-grown Ge NWs using Au catalyst particles with diameters of 20, 40, and 80 nm. The authors observed two distinct, defect-free kinking modes (Figure 11a,b). For diameters of ∼20 nm, the NW growth axis changed from vertical [111] to ⟨110⟩. According to the authors, this observation agrees with the phase field simulations that show a spontaneous transition from ⟨111⟩ to ⟨110⟩ at this diameters. Thicker NWs kinked from [111] to an inclined ⟨111⟩ axis. The authors link this to an error in sidewall facet development that leads to a contraction of the (111) growth facet area as NW grows, resulting in an instability of the Au−Ge droplet at the tip of the NW.[37] Moreover, the probability of kinking at different tested temperatures strongly depended on the catalyst size (Figure 11c).

Sometimes the catalyst is applied on the substrate in the form of a thin film. Wacaser et al.[72] examined the supercooled VLS growth of silicon NWs on Si substrates with thin aluminum films. The authors varied the thickness of the Al layer, which clearly influenced the NW diameters, the density of vertically aligned epitaxial NWs, and the density of other growth irregularities, including kinks. It was found that optimal growth conditions for vertically aligned NWs were achieved at a 5 nm Al

https://doi.org/10.1021/acs.cgd.1c00802
Cryst. Growth Des. 2022, 22, 871−892

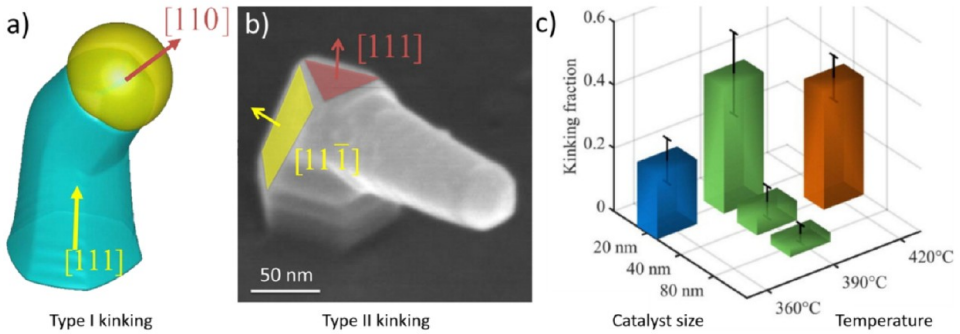

Figure 11. (a,b) Two types of kinking observed in experiments. (c) Dependence of the kinking probability at different tested temperatures on the catalyst size. Adapted from ref 37. Copyright 2016 American Chemical Society.

layer thickness. For thinner Al layers, the density of aligned NWs decreased, and many NWs deviated from vertical growth and kinked.

Wen et al.[70] studied the CVD growth of copper-catalyzed silicon NWs on a copper-coated Si substrate at around 500−600 °C. They used TEM to observe the NW growth mechanism directly and quantify the growth kinetics of individual wires. The authors found that the growth direction of individual NWs is related to the orientation and shape of the catalyst, leading to a rich morphology and extensive kinking (about 50% of the observed NWs).

Potts et al.[83] further advanced the techniques of catalyst manipulation. They demonstrated an unusual kinking method for achieving L-shapes in self-catalyzed InAs and InAsSb NWs, by *in situ* formation and manipulation of indium droplets obtained either by annealing NWs in vacuum or by direct deposition on the NWs. The authors demonstrated that the size and position of indium droplets can be tuned by changing the annealing time. The indium droplets were then used as seed particles to initiate growth in different crystallographic directions. Depending on the position of the seed, linear or L-shaped nanostructures were obtained. The authors then further investigated the formation of droplets by annealing L-shaped structures. They observed different positions of the indium droplets and different shapes of nanostructures including thicker L-shaped structures, longer branches, and nanobridges. The latter is particularly interesting as the second section of the NW that is formed after the second annealing step grows toward ⟨111⟩, which is a quite untypical direction for self-catalyzed arsenide NWs.

The probability of kinking strongly correlated with the NW diameters for catalyst-free synthesis methods as well. For instance, Ge NWs grown in the unseeded organic vapor-phase-based process at 420 °C were mostly straight with diameters in the range of 7−20 nm and large aspect ratios.[49] A small percentage of the NWs had a larger average diameter (up to 50 nm) and higher diameter variance, with a considerable degree of kinking.

Growth Rate. The degree of kinetic forcing required to induce kinking is different for different materials and therefore can depend on the growth rate, which is often regulated by the precursor flow rate in the chamber. For example, Ge NWs kink at much larger kinetic force than Si, and therefore, Ge NWs grown at $T = 300$ °C do not kink at growth rates below 5 nm/sec, while Si NWs grown at 400 °C kink already at a growth rate of 1 nm/sec.[64] For III−V materials, the ratio between the molar flow rates of the group V and group III precursors (V/III ratio) can considerably influence the morphology of NWs.[42,110,114,115] For instance, kinking in GaAs NWs was observed in Au-catalyzed MOCVD when a V/III ratio exceeded 90.[110] Dayeh et al.[58] studied the VLS growth of Au-catalyzed hybrid Ge−Si NWs with a precise control over the growth conditions. The authors observed a 19.5° kinking at higher Si growth rates resulting from twin boundary formation. As the twin boundary propagates into the NW, it locally increases its diameter and disturbs the liquid growth seed, increasing the line tension that is restored by switching the growth direction from a ⟨111⟩ to ⟨211⟩. The occurrence of such stacking faults was shown to decrease by reducing the growth rate.

Etching. In a few works, kinked NWs were prepared by etching—a method that is fundamentally different form the VLS and VSS processes. For instance, in a recent study, Chen et al.[92,116] prepared kinked Si NWs by alternating metal-assisted chemical etching. First, patterns were formed from polystyrene microspheres on a (100)-oriented single-crystalline Si substrate through a self-assembly process. Then, Ti and Au films were deposited on Si as catalysts. Next, straight NWs were formed by immersing the Si substrate into etchant A, which consisted of deionized water, H_2O_2, and hydrofluoric acid. Then, the substrate was removed from etchant A and immersed into etchant B, which contained also glycerol. The etching directions were different in the two etchants, which led to kink formation at the joints of different crystallographic directions. The straight and slanted etching directions were [100] and [211], respectively. By repeating the etching procedures A−B−A−B−A, multikinked Si NWs were fabricated, consisting mainly of three straight segments and two segments slanted at an angle of 54.8°.

A similar technique was used by Sandu et al.,[117] who synthesized kinked Si superstructures with aspect ratios above 200. They used metal-assisted chemical etching of a Si substrate via a patterned Au mask, as shown in Figure 12. To form the kinks at the desired location, Si etching was interrupted at specific times by submersing the sample in methanol. The angles of the kinks were found to be dependent on the size of the openings in the Au catalyst.

The advantage of the described etching protocols is that they enable to control the number, angle, and location of the kinks via sequential etch−quench sequences.

Summary of modulation parameters. Based on the examined literature, we can draw some conclusions regarding the efficiency of the different methods in obtaining kinked NWs of a desired geometry. Although modulating the temperature during the synthesis is the simplest way to achieve kinks, it is not

https://doi.org/10.1021/acs.cgd.1c00802
Cryst. Growth Des. 2022, 22, 871−892

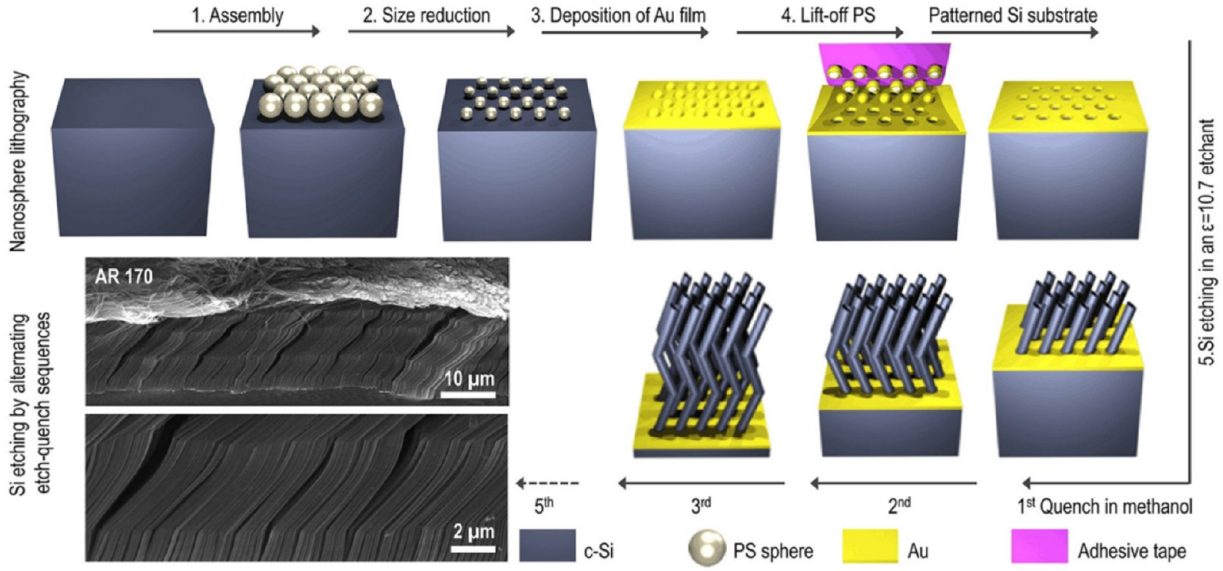

Figure 12. Schematics of the synthesis of kinked Si NWs 200 by metal-assisted chemical etching of Si substrate. First, the Si substrate is patterned with a holey Au mask by polystyrene nanosphere lithography. Second, the nanostructuring of Si follows repetitive etch−quench sequences. The SEM pictures show the k-kinked Si NWs that resulted after five successive etch−quench sequences. Adapted from ref 117. Copyright 2019 American Chemical Society.

the most efficient method for the production of kinked NWs if high quality and good control over the location of the kink and the geometry of the kinked NWs is needed. Kinking that occurs when the growth temperature is outside of the optimal range required for straight vertical growth is unpredictable and can be considered more like a random defect. Moreover, changing the temperature of the whole reactor is rather time-consuming. The situation is even more complicated by the fact that the precise control and measurement of the temperature at the sample site with sufficient precision and reliability is not trivial.

Pressure modulation is significantly faster, gives better control, and can lead to a higher quality of the kinked NWs, compared to temperature modulation. However, based on the available literature, it seems that the applicability of precursor pressure modulation is very limited in terms of material choice and so far is used mainly for production of kinked Si NWs. This is also the case for kinking achieved by anisotropic etching that has good control over the process but is limited mainly to silicon.

Regulating the growth rate by controlling the precursor flow is another simple method that, however, can suffer from a compromised quality, as increased flow rates lead to defects like stacking faults. The highest flexibility is obtained when the composition of the gas in the chamber is modulated during the synthesis in a controllable manner, following the well-elaborated recipes available in dedicated literature. Such an approach allows synthesis of high-quality long multikinked NWs, with various geometries and compositions, including heterostructured ones. Gas composition modulation can be combined with other methods when needed, for even more advanced control over the process. Therefore, we can conclude that in most cases, composition modulation is the preferable method for achieving kinked NWs in a well-controllable manner. However, some materials may benefit from the simplicity of other methods, like pressure modulation for Si NWs.

In order to have a better overview of the materials and methods analyzed in the present work, we summarized some relevant data in Table 1. The synthesis method alongside with the parameter that should be modulated to achieve kinking are shown for each material and its corresponding crystal structure. We also added data on the growth directions and kinking angles observed in the studies that were analyzed.

PREVENTING KINKS

Considering that for most situations kinking is an undesirable effect, we would like to briefly summarize some of the aspects of the synthesis process that are essential for achieving kink-free NWs.

First of all, growth conditions should be chosen carefully, as often straight kink-free NWs can be achieved only in a narrow range of temperatures and pressures.[93] Two distinct scenarios have been reported in the literature—depending on the system and method, kinking may happen either at "lower-than-optimal" or "higher-than-optimal" growth temperatures. In some studies,[118] a two-temperature growth technique with separate nucleation and growth temperatures was applied to achieve kink-free vertical NWs. Choosing the proper temperature for synthesis does not yet guarantee kink prevention. For instance, Song et al.[101] observed kinking near the base in epitaxial Ge NWs at any temperature in the range required for synthesis (from 300 to 380 °C). However, kinking was more prominent for NWs grown at higher temperatures, indicating that at least minimization of kinking is still possible. Fortuna et al.[42] emphasized the importance of maintaining the stability of the catalyst and the NW−catalyst interface through isothermal growth techniques to avoid kinking and other unwanted defects. Precursor flow rates, as well as composition, should also be kept in the optimal range. For instance, it was demonstrated[110] that a high ratio of group V to group III precursors dramatically improves the quality and purity of GaAs NWs. However, a further increase of the V/III ratio leads to kinking and increases NW tapering.

Since the appearance of kinks was shown to be dependent on the size of the catalyst particle,[62] the diameter of the catalyst should be chosen correspondingly to avoid kinking. Composition of the catalyst is another factor that can play an important role in the growth direction of NWs. Wang et al.[112]

https://doi.org/10.1021/acs.cgd.1c00802
Cryst. Growth Des. 2022, 22, 871−892

Table 1. Most Frequent Kink Directions in Nanowires

material	structure	method	modulation parameter	growth and kink directions	angle deg
Si	diamond cubic	VLS (most works)	pressure[45,47,48,65,73,102]	110 ↔ 111	71, 90, 109, 125, 130, 141, 160
		chemical etching[92,116,117]	pressure and temperature[64,67,103]	110 ↔ 112	
			vapor/gas composition[41,77,103]	112 ↔ 111	
			size factor[56,64,70,72]	112 ↔ 110 ↔ 112	
				111 ↔ 331	
Ge	diamond cubic	VLS (most works)	temperature,[49,101,104]	110 ↔ 111	35, 70, 60, 90, 120
		seedless MOCVD[49]	vapor/gas composition[104]	110 ↔ 112	
			size factor[37,49,62]		
GaAs	zinc blende (ZB)	VLS[51,110]	vapor/gas composition[110]	101 ↔ 110 ↔ 011	45, 60, 90
			growth rate[110]	[111]B ↔ non-[111]B	
GaSe	wurtzite (WZ)	VLS[52]	temperature[52]	11−20 ↔ 2−1−10	120
InP	ZB and ZB/WZ mix	VLS[112]	vapor/gas composition[112]	100 ↔ 111	16, 55
InAs	WZ ↔ ZB	MBE[113]	vapor/gas composition[113]	000−1 ↔ 00−1	no data
			size factor[83]		
CdS	WZ	VLS[41]	vapor/gas composition[41]	11−20 ↔ 11−20	120
SnO_2	rutile	VLS[123]	spontaneous[123]	001 ↔ 211	123
heterostructure	material-dependent	VLS	vapor/gas composition[47,53,58,59,63]	material-dependent	

demonstrated the high (97%) yield of vertical ⟨100⟩-oriented InP NWs when the Au catalyst droplet was filled with In prior to NW nucleation to the equilibrium composition during VSL growth. Otherwise, the shape of the droplet changes during the nucleation process due to the uptake of In, which disturbs the growth. Prefilling the catalyst with In brought it into equilibrium conditions, and ⟨100⟩ growth was stabilized. If the In content will be too high, the NW will first kink to one side to release excess material and then start to grow. Therefore, optimization is important.

For heterostructured NWs (GaP/Si, GaAs/Ge, and GaAs/S), the interlayer between segments can enable the growth of unkinked hybrid NWs.[56] Dayeh et al.[58] found for the VLS synthesis of Au-catalyzed Ge−Si NWs that maintaining a liquid Au particle with high supersaturation is required to initiate the epitaxial growth of a Si segment on the previously grown Ge NW, to stabilize the Au seed on top of the NW, and prevent kinking.

Finally, considering that kinking is often attributed to interactions at NW/catalyst interface, choosing a catalyst-free method like, for example, MBE over CVD when possible can help achieving straight nanowires.[119]

PROPERTIES AND APPLICATIONS OF KINKED NWS

Kinks are expected to influence the properties and behavior of NWs. However, the extent of the impact strongly depends on the type of kink, i.e., whether it involves defects and/or change of crystallographic direction. It is evident that these factors are crucial for the mechanical strength and propagation of phonons or charge carriers inside a NW. Although the number of studies related to kinked NWs is rather large, most of them are dedicated only to synthesis, with far less including measurements of their properties and/or discussion on the applications of kinked NWs. Here, we overview some of the works that go beyond synthesis and include measurements or simulations of some of the properties of kinked NWs.

Mechanical. The mechanical properties of kinked NWs can play an important role in the operation of nano-electro-mechanical devices. For now, most studies in this direction are done using computer simulations, as experimental measurements are challenging. For instance, Jiang and Rabczuk[55] performed classical molecular dynamics (MD) simulations to demonstrate the application of kinked silicon NWs as nanoscale springs. Spring-like oscillations in a GHz frequency range were actuated in kinked NWs of various aspect ratios, using a procedure similar to the actuation of a classical mass spring oscillator. Using energy spectrum analysis, the authors detected spring-like mechanical oscillations as well as some other low-frequency oscillations. They obtained a dimensional crossover (from one-dimensional to three-dimensional) of the transverse oscillation mode as the aspect ratio of the kinked NWs decreased.

Jiang et al.,[54] performed both MD simulations and finite element method (FEM) beam model calculations to investigate the elastic properties of kinked (zigzag) silicon NWs. The Young's modulus was found to be highly sensitive on the arm length, with a dependence of the functional form $Y = c_1/(b + c_2)$, where b is the arm length and $c_{1,2}$ are coefficients that depend on the material and the geometry of the kinks. This dependence was derived via a simplified model that represents the kinked NWs as a series of springs, which replace both the elastic arms and angles. Still, they gave excellent agreement with MD simulation results, demonstrating the spring-like elastic properties of kinked Si NWs.

Furthermore, MD simulations performed by Jing et al.[120] demonstrated that kinked silicon NWs have a much larger fracture strain compared to straight ones, as shown in Figure 13. For the symmetric structure (left diagram), it was found that the fracture stress decreased with the periodic length, while the fracture strain abruptly increased to large values and then stabilized. Note here that $L = 0$ corresponds to a straight NW. For the asymmetric case (right diagram), the fracture stress did not significantly depend on the arm length L_{arm} in contrast to the fracture strain that increased monotonically with L_{arm}. The authors concluded that kinked Si NWs with a larger fracture strain can be a promising anode material in high-performance Li-ion batteries, since the Si anode can swell by a large factor during initial lithiation.

Chen et al.[92] studied the effect of kinks on the mechanical properties of silicon NWs, using MD simulations, indirectly validated by experiments. The authors found that kinks are weak points in the NW. They also calculated the elastic modulus of

https://doi.org/10.1021/acs.cgd.1c00802
Cryst. Growth Des. 2022, 22, 871−892

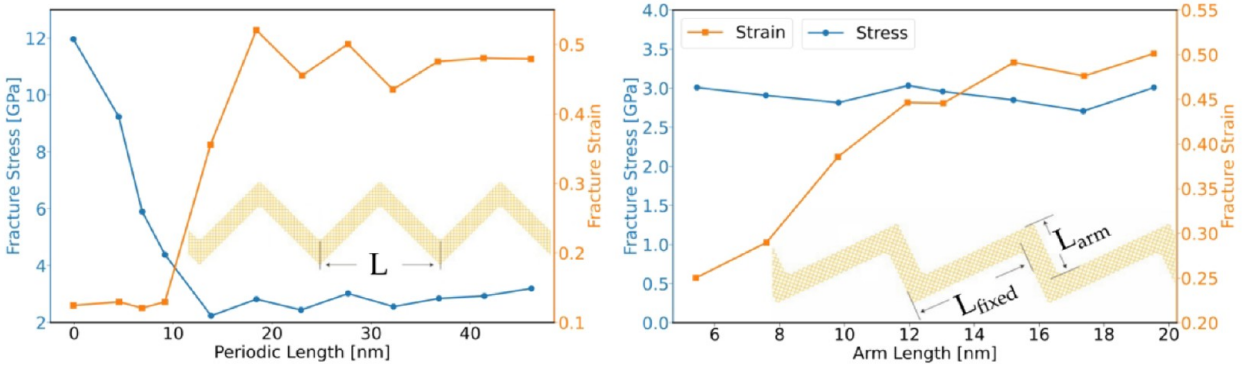

Figure 13. Fracture stress (left axes, blue dot markers) and fracture strain (right axes, orange square markers) as a function of the periodic length L in symmetric zigzag kinked Si NWs (left diagram) and the arm length L_{arm} in asymmetric ones with L_{fixed} = 19.5 nm (right diagram). The NW configurations for each case are shown in the insets. Data are from ref 113.

kinked NWs, finding it significantly smaller (~30 GPa) compared to a straight NW (~106 GPa), in line with the findings of ref 54. Moreover, in the experiments by Chen et al., the kinked NWs fractured at kinks under load.

Finally, Jiang[121] performed a lattice dynamical study of intrinsic out-of-plane twisting vibrations that are self-generated in zigzag-shaped kinked Si NWs to withstand the out-of-plane mechanical instability. The authors explored the effect of kinking on the phonon spectrum of the NWs and obtained an analytical formula for the geometrical (cross-sectional area and the arm length at given temperature) dependence of the twisting amplitude of the kinked Si NWs. The result provides valuable information on the kinking-induced twisting stability of kinked NWs when used as bioprobes for intracellular recording application.

Thermal. Jiang et al.[38] performed MD simulations to investigate the reduction of the thermal conductivity by kinks in silicon NWs. According to their results, the reduction can achieve 70% at room temperature. The thermal conductivity was found to be insensitive to the temperature, since the heat transport is mainly limited by the phonon scattering at the kink interface. Two mechanisms responsible for the reduced thermal conductivity were proposed: (1) the interchange between the longitudinal and transverse phonon modes and (2) the pinching effect, which is a new type of localization for the twisting and transverse phonon modes in the kinked silicon NWs. The authors demonstrated that these kink-induced effects offer a novel and effective approach for modulating heat transfer in NWs, making the kinked silicon NWs a promising candidate for thermoelectric materials.

The first experimental demonstration of the kink thermal resistance was reported in a recent study by Zhang et al.[122] They found a 15−36% reduction of thermal conductivity in kinked boron carbide NWs compared to straight ones, which is up to ~7 times more pronounced than the effect predicted by Juang et al.[38] in the MD simulations (if the results are normalized to the investigated size accordingly). The authors attributed this effect to the high thermal resistance of the kinks, estimated to be ~30 times that of a straight wire segment with a length equivalent to that of the kink's central line. According to TEM studies, the kinked regions were all single-crystalline and defect-free. Therefore, the reduced thermal conductivity cannot be attributed to low a structural quality at the kinks, but it is rather related to the kinked morphology itself. Furthermore, larger diameter NWs were generally found to have higher kink resistance. This might be due to the weaker boundary scattering from the NW surface in larger wires. In addition to defect-free kinks, some NWs had kinks with clear structural defects, which were oriented in parallel to the stacking faults in one of their legs. Surprisingly, the thermal conductivity of such NWs was higher than that of comparable NWs with defect-free kinks but still lower than that of straight wires. This contradicts the well-known fact that defects can scatter phonons and obstruct their transport. In order to get a deeper understanding of the observed phenomena, the authors performed a Monte Carlo (MC) simulation of phonon transport through an "L"-shaped kink and concluded that the highly focused phonons have to undergo scattering to make the turn and enter the opposite leg of a kink. More scattering events in the kink assist the change of phonon direction and thus reduce the kink resistance. These findings provide valuable data for the accurate thermal management of nanoelectronic devices that involve kink-like wire morphologies.

Further insights on the phonon transport in kinked NWs can be found in a recent study of Zhao et al.,[40] who performed nonequilibrium MD studies of thermal transport through kinked and straight Si NWs. They confirmed that kinks lead to lower (up to 1.6 times) thermal conductivity for kinked NWs compared to straight ones, by reflecting phonons back into their incoming arms. The decrease in thermal conductivity becomes more pronounced as the arm length increases. However, when heavier isotope atoms were introduced in the kink region, simulations replicated the experimental observation that defects in the kink region can in fact facilitate thermal transport through deflecting phonons into the adjacent arm.

Electronic. Similar to the situation with phonons, kinks are expected to cause resistance on the propagation of charge carriers in semiconducting NWs. However, as was shown by Cook and Varga[39] in their first-principles transport calculations, the conductance strongly depends on the kink geometry. For certain geometries, the conductance of the kinked NWs is close to that of the ideal wire, due to the introduction of resonance states. Moreover, kinked NWs with larger diameters are expected to be better conductors, as there are more conduction channels available and the perturbation induced by the kink has a lesser effect.

There are also experimental studies available. For instance, Tian et al.[41] demonstrated and characterized topologically defined nanoelectronic devices based on kinked semiconductor NWs by combining precisely controlled 120° kinking with additional modulation of the dopant, to modify the electronic properties of NWs in a well-defined manner. Figure 14 represents the characterization of a kinked Si NW with

https://doi.org/10.1021/acs.cgd.1c00802
Cryst. Growth Des. 2022, 22, 871−892

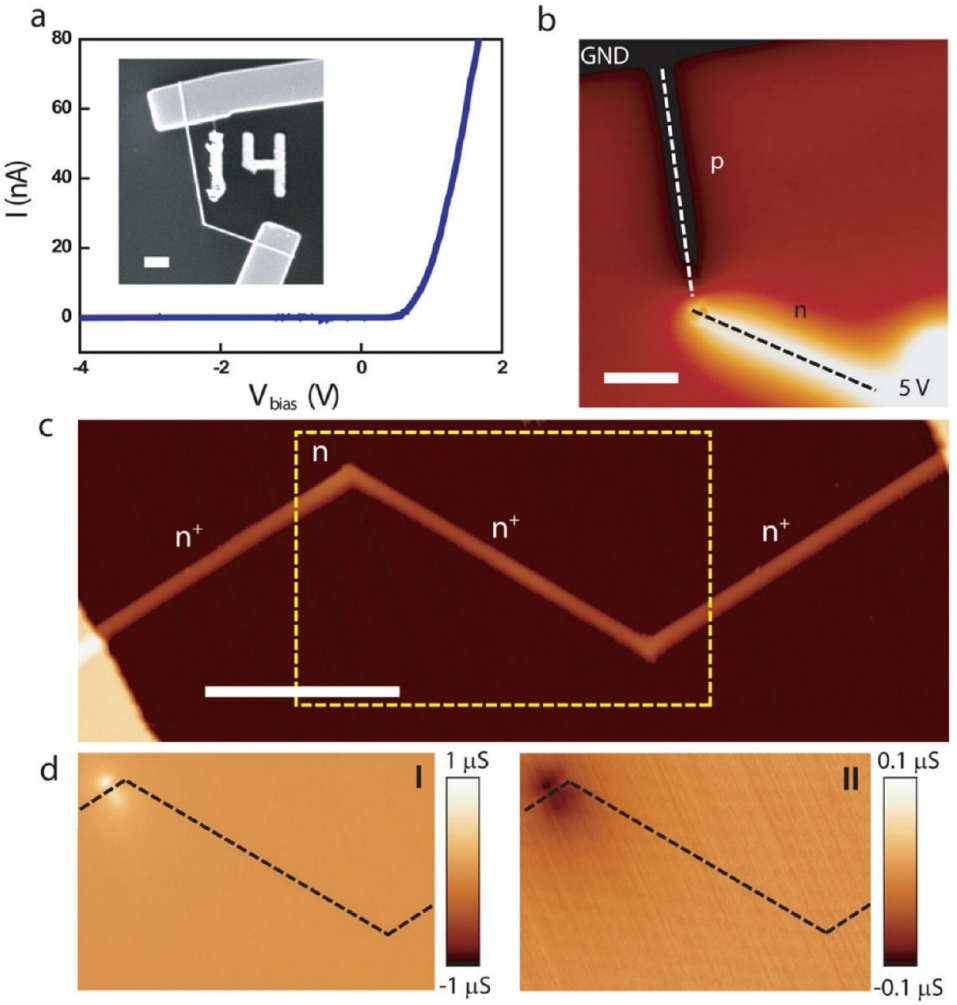

Figure 14. (a) $I-V$ data recorded from a kinked p−n silicon NW-based device. Inset: SEM image of the device structure. Scale bar is 2 μm. (b) Electrostatic force microscopy image of a p−n diode reverse-biased at 5 V. The atomic force microscope (AFM) tip voltage was modulated by 3 V at the cantilever-tip resonance frequency. The signal brightness is proportional to the NW device surface potential and has an abrupt drop around the kink position. The dashed lines indicate the NW position. Scale bar is 2 μm. (c,d) AFM and scanned gate microscopy (SGM) images of one n+−kink−n+−kink−(n−n+) dopant modulated double-kinked silicon NW structure. The scale bar in (c) is 2 μm. The SGM images were recorded with a V_{tip} of 10 V (I) and −10 V (II), respectively, and a V_{sd} of 1 V. The dark and bright regions correspond to reduced and enhanced conductance, respectively. The black dashed lines denote the NW position. Reprinted with permission from ref 41. Copyright 2009 Springer.

integrated n- and p-type arms that was synthesized by switching phosphine and diborane dopants during the Au-catalyzed VLS growth sequence. The current−voltage ($I-V$) data (Figure 14a) reveal a current rectification in reverse bias with an onset at a forward bias voltage of ∼0.6 V, consistent with the synthesis of a well-defined p−n diode within the kinked structure. According to the electrostatic force microscopy (EFM) characterization of the kinked p−n NW in reverse bias (Figure 14b), the voltage drop occurs primarily at the p−n junction, localized by the kink during growth.

This concept can be extended to the design of NWs with a distinct functionality at sequential kinks. Scanned gate microscopy (SGM) data (Figure 14d) acquired from the area denoted on the atomic force microscopy image (Figure 14c) reveal increased (decreased) NW conductance as the SGM probe with positive (negative) gate potential is scanned across the n-type segment adjacent to the upper-left kink junction. This confirms the integration of an n-type field-effect transistor (FET) at a well-defined and recognizable location of the structure. The absence of a gate response from the lower-right kink junction suggests that the single-crystalline kink structure itself will not alter the electronic transport properties of the NW. The authors stated that their results significantly contribute to the realization of ab initio designed and "self-labeled" 2D NW structures and may initiate applications in the bottom-up integration of active devices in nanoelectronics, photodetector arrays, and multiplexed biological sensors and the development of multiterminal 3D nanodevices.

Utilization of kinked structures in fabrication of FETs was reported also by Shen et al.[79] for In_2O_3 NWs grown by Au-catalyzed CVD. The authors report n-type conductivity with mobilities exceeding 200 cm2/(V·s), opening a route for fabricating high-performance electronic and optoelectronic devices. The synthesized nanostructures demonstrated ultrafast photoinduced reversible wettability, switching from hydrophobic to superhydrophilic in 14 min.

Potts et al.[83] studied the electrical properties of L-shaped kinked nanostructures grown by the annealing method (see details of Potts et al. above) using two-point electrical measurements. The conductivity of the nanostructures (81 ±

https://doi.org/10.1021/acs.cgd.1c00802
Cryst. Growth Des. 2022, 22, 871−892

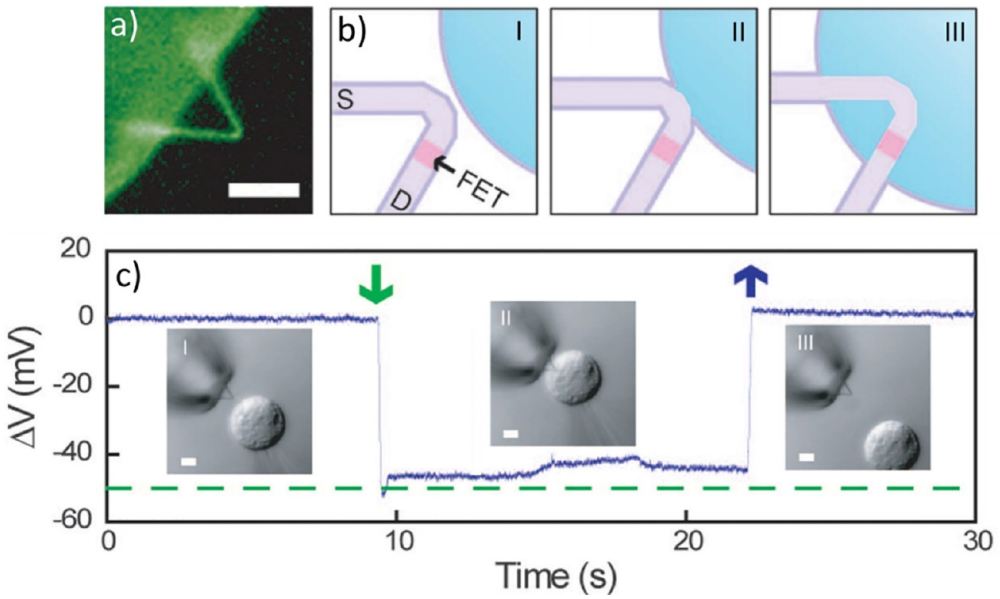

Figure 15. Surface modification and cellular entry. (a) Fluorescence image of a lipid-coated NW probe. (b) Schematics of NW probe entrance into a cell. Dark purple, light purple, pink, and blue colors denote the phospholipid bilayers, heavily doped NW segments, active sensor segment, and cytosol, respectively. (c) Differential interference contrast microscopy images and electrical recording of an HL-1 cell and 60° kinked NW probe as the cell approaches (I), contacts and internalizes (II), and is retracted from (III) the nanoprobe. A pulled-glass micropipette (inner tip diameter ≈ 5 mm) was used to manipulate and voltage clamp the HL-1 cell. The dashed green line corresponds to the micropipette potential. Scale bars are 5 mm. Reprinted with permission from ref 44. Copyright 2010 American Association for the Advancement of Science.

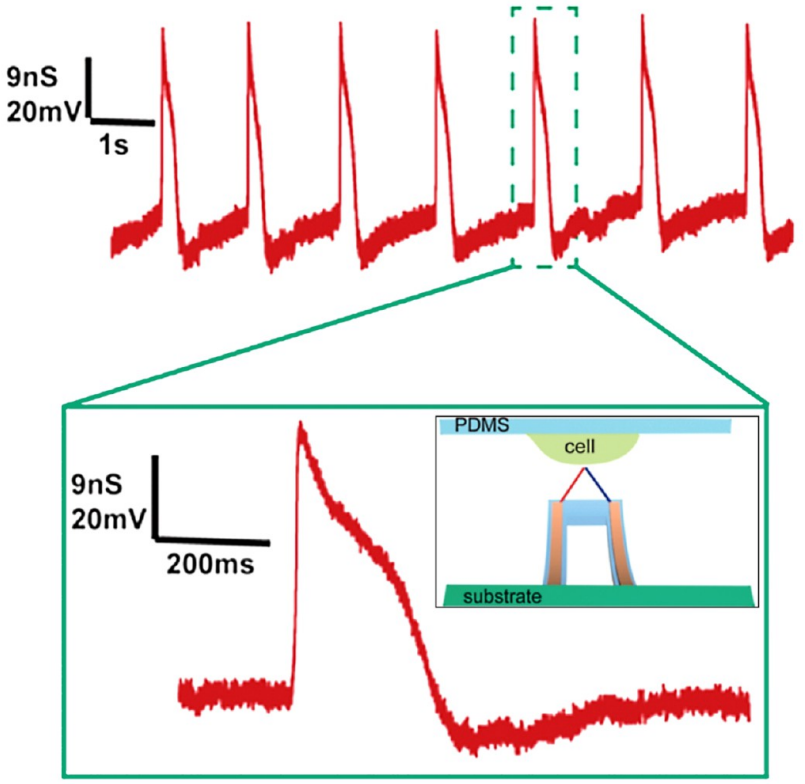

Figure 16. Intracellular electrical recording from spontaneously beating chicken cardiomyocytes. (Top) Steady state intracellular recording using 3D kinked p−n nanoprobes from a spontaneously beating cardiomyocyte cell. (Bottom) Zoom of the single-action potential peak from the green-dashed region. Inset: Schematic of intracellular recording from spontaneously beating embryonic chicken cardiomyocytes cultured on PDMS substrate using 3D kinked p−n nanoprobes. Adapted from ref 53. Copyright 2012 American Chemical Society.

23 S cm^{-1}) was found to be comparable to standard ⟨111⟩B plane self-catalyzed InAs NWs. All parts of the investigated device exhibited an n-type gate response, although the intensity of the response varied significantly.

https://doi.org/10.1021/acs.cgd.1c00802
Cryst. Growth Des. 2022, 22, 871−892

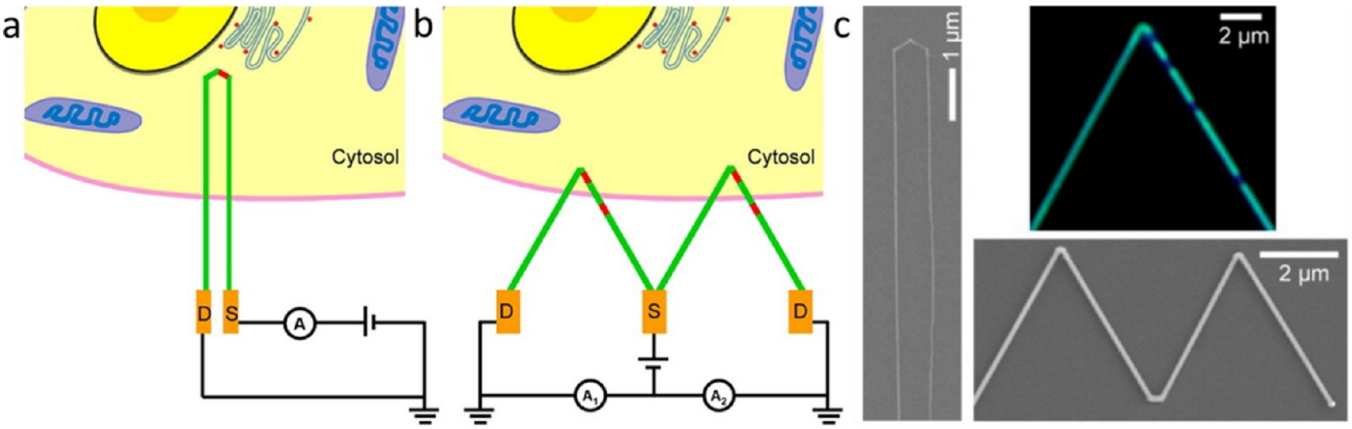

Figure 17. (a,b) Overview of designs and potential applications of kinked NWs. (a) U-shaped NW with integrated nanoFET (red) shown as a bioprobe for intracellular recording. (b) W-shaped NW with multiple nanoFETs (red) illustrated as a bioprobe for simultaneous intracellular/extracellular recording. Green color indicates heavily doped (n++) nanoelectrode arms, red indicates the point-like active nanoFET elements, and gold indicates the fabricated metal interconnects. A schematic of a cell to scale is drawn with the different device designs to show the potential for achieving minimally invasive deep penetration (a) and multiplexed intracellular and extracellular recording (b). (c) U- and W-shaped NWs synthesized in the study. Upper right image is the dark-field optical microscopy image of a KOH-etched kinked NW with four nanoFETs. The dark segments correspond to the four lightly doped nanoFET elements. Adapted from ref 45. Copyright 2012 American Chemical Society.

Gan et al.[123] compared the efficiency of straight and kinked SnO_2 NWs in photodetector applications and found a significant enhancement of the local electric field at the kink, which improves the electron−hole separation efficiency and the transmission time of the carrier, thus improving both the photocurrent and response time of the SnO_2 NW.

Biological. Nanoelectronic devices made of various nanostructures including NWs offer substantial potential for studying biological systems. FETs based on semiconductor NWs and other semiconducting nanostructures have been extensively studied as biological/chemical (bio/chem) sensors for many years.[53] High sensitivity was demonstrated for one- and two-dimensional sensors. However, most works were focused on planar device designs, while the realization of ultimate point-like and 3D detectors remains challenging. Kinked NWs may help to overcome this limitation.

Superstructures made of kinked NWs have been utilized to fabricate 3D bend-up nanoelectronic probes for recording extra- and intracellular action potentials from single cells and tissues.[44,45,53] For instance, Tian et al.,[44] using the synthesis method described in ref 41, presented the concept of synthetic integration of a nanoscale FET (nanoFET), localized by modulating the doping at the tip of an acute-angle kinked Si NW. At this location, nanoscale connections are made by the arms of the kinked NW, and remote multilayer interconnects allow a 3D probe operation (Figure 15). 3D nanoFET probes exhibited electrical conductivity and high pH sensitivity in aqueous solution, independent of severe mechanical deflections. According to the authors, 3D nanoprobes, if modified with phospholipid bilayers, can enter single cells allowing recording of intracellular potentials.

In another study,[53] the same team discussed the advantages of nanoscale p−n diodes, described in details in their earlier work,[41] in bio- and chemosensing applications. The nanoscale axial p−n junctions were synthetically introduced at the joints of kinked Si NWs. Electrical transport measurements revealed a rectifying behavior with well-defined turn-on in the forward bias, in accordance with expectations for a p−n diode. Scanning gate microscopy measurements demonstrated that the most sensitive region was localized near the kink at the p−n junction. High-spatial-resolution sensing of fluorescent charged polystyrene nanobeads was carried out using p−n diode probes in aqueous solution. Multiplexed electrical measurements with simultaneous confocal imaging demonstrated detection of single nanoparticles. In addition, kinked p−n junction NWs configured as 3D probes demonstrated the capability of intracellular recording of action potentials from electrogenic cells. The probes were functionalized with 1,2-dimyristoyl-*sn*-glycero-3-phosphocholine (DMPC). Embryonic chicken cardiomyocyte cells cultured on a polydimethylsiloxane (PDMS) substrate were then positioned over an NW probe. Next, the probe was inserted into the cell, and the evolutions of its conductance were recorded successfully, registering the signal from a spontaneously beating cardiomyocyte cell (Figure 16).

Further development in this field was done by Xu et al.,[45] who substantially expanded the scope of functional building blocks made of kinked NWs, through the ab initio design and synthesis of several new structures. They demonstrated spatially isolated point-like nanoelectronic probes made of kinked Au-catalyzed VLS-grown Si NWs. Their structures are especially useful for monitoring biological systems where a precisely engineered size and structure are highly desired. The authors presented three types of novel functional kinked NWs:

(1) Zero-degree kinked nanostructures with two parallel heavily doped arms of U-shaped structures, where three 120° kinks can define the "U" shape. A nanoFET detector is formed at the tip of the "U" by modulating the doping between two of these kinks. The heavily doped arms before and after the three kinks function as a source and drain (S−D), respectively. The width of this U-shaped element is determined by the interkink segment lengths and is independent of the arm length. This design should allow a deep penetration of the nanoFET detector into cells and tissue, without increasing its cross-sectional area.
(2) Series multiplexed functional kinked (at 120°) NWs, integrating multiple nanoFETs along the arm and at the tips of V-shaped structures.
(3) Parallel multiplexed kinked NWs integrating nanoFETs at the two tips of W-shaped nanostructures with 120° kinking angles.

https://doi.org/10.1021/acs.cgd.1c00802
Cryst. Growth Des. 2022, 22, 871−892

The authors succeeded to synthesize U-shaped kinked NWs with a distance between parallel arms of just 650 nm. One of the arms/tip of V-shaped and distinct arms/tips of W-shaped NWs were encoded with multiple nanoFETs during synthesis. NWs were then assembled into 3D nanoFET probes. (Figure 17)

Synthesis and design of p−n junction devices based on the kinked NWs described above greatly contribute to a growing array of methods and building elements for fabrication of highly compact and multiplexed 3D nanoprobes with highly localized sensing regions for applications in life sciences. They hence open substantial opportunities in areas ranging from bio- and chemosensing, nanoscale photon detection, to 3D imaging from within living cells and tissue.[53]

Structural. Kim et al.[86] have formed nanobridges by using single-kinked Ge NWs on uncommon V-grooved (100) Si substrates to take advantage of their vertical (111) sidewalls,[124] without resorting to the noncompatible (110) substrate. This is another example that reveals the potential of kinked NWs as promising building blocks for future devices. However, according to the authors,[86] the control of the crystallographic direction of segments in multiply kinked NWs still remains a challenging issue to be solved.

SUMMARY AND OUTLOOK

Kinking in NWs (i.e., abrupt changes in NW growth directions) is a phenomenon that has been known to scientists for decades. However, in recent years, kinking has attracted increased attention and is now considered a powerful tool for additional tweaking of the properties and geometry of one-dimensional nanostructures. To gain comprehensive control over the kinking process and utilize kinked NWs for practical applications, a thorough understanding of the kinking mechanisms is critical. As was shown in the present Review, there is a wide range of factors that may affect the NW growth direction, including the growth temperature, pressure, precursor composition, substrate orientation and treatment, NW diameter, catalyst size, etc. Moreover, these factors are often interconnected. The resulting growth direction is determined by the energies of the NW surface facets, NW−catalyst interface, and the availability of nucleation sites.[42] Some of the parameters can be tailored during the synthesis, leading to a change of the growth direction of already growing NWs, thus resulting in kinked structures. There are also several different mechanisms that lead to the NW kinking. Depending on the conditions and materials, one or another mechanism may prevail.

The properties of kinked NWs strongly depend on the type of kinking. Depending on various factors, the whole kinked NW may have the same crystallographic orientation, or kinking can involve a change in the crystallographic orientation. Kinks are often accompanied by crystallographic defects; however, defect-free kinking is also observed. NWs can have single or multiple kinks.

Despite a considerable amount of studies dedicated to kinking in NWs, there is still a lot to contribute. The majority of studies are dedicated to kinking of Si NWs in the VLS growth processes, while other materials and methods are significantly less exploited. Moreover, the number of studies that involve characterization of kinked NWs that extends beyond simulations or routine microscopy and spectroscopy is very limited. Even less studied are potential applications of kinked NWs. The most exploited and promising field seems to be the utilization of kinked NWs as nanoscale sensors in biological applications: various operational prototypes are already demonstrated in several recent studies. Extension of research to other materials and potential applications in various areas with corresponding characterization of mechanical, electrical, thermal, and other properties is a real challenge and has to be further explored.

AUTHOR INFORMATION

Corresponding Author

Sergei Vlassov − *Institute of Physics, University of Tartu, 50412 Tartu, Estonia;* orcid.org/0000-0001-9396-4252; Email: sergei.vlassov@ut.ee

Authors

Sven Oras − *Tallinn University of Technology, Tartu College, Tartu 51008, Estonia; Institute of Technology, University of Tartu, 50411 Tartu, Estonia*

Boris Polyakov − *Institute of Solid State Physics, University of Latvia, LV-1063 Riga, Latvia;* orcid.org/0000-0002-6626-1065

Edgars Butanovs − *Institute of Technology, University of Tartu, 50411 Tartu, Estonia; Institute of Solid State Physics, University of Latvia, LV-1063 Riga, Latvia;* orcid.org/0000-0003-3796-1190

Andreas Kyritsakis − *Institute of Technology, University of Tartu, 50411 Tartu, Estonia*

Veronika Zadin − *Institute of Technology, University of Tartu, 50411 Tartu, Estonia*

Complete contact information is available at: https://pubs.acs.org/10.1021/acs.cgd.1c00802

Notes

The authors declare no competing financial interest.

Biographies

Sergei Vlassov (born in 1980) is an associate professor at the Institute of Physics, University of Tartu (Estonia). He received an MSc in applied physics (2007) and PhD in material science (2011) in the University of Tartu (Estonia) and then spent 2 years as a postdoc in the Institute of Solid State Physics, University of Latvia. His research interests are mainly related to experimental studies of mechanical and structural properties of individual nanostructures. By the spring of 2021, Sergei has 85 publications in the Google Scholar database, with an h-index of 19.

https://doi.org/10.1021/acs.cgd.1c00802
Cryst. Growth Des. 2022, 22, 871−892

Sven Oras (born in 1989) has a PhD in Materials Chemistry (2018, University of Upper Alsace) and a Master's Degree in Physics (2014, University of Tartu). His research activities are focused on the experimental characterization of nanostructures focusing mainly on mechanical and tribological properties. In the MATTER project, Sven is a postdoc responsible for performing nanomanipulation experiments inside a scanning electron microscope (SEM) affecting single nanostructures and performing characterization of nanostructures with an atomic force microscope (AFM). By the end of 2020, Sven has 15 publications in the Google Scholar database, with an h-index of 8.

Boris Polyakov is a senior researcher in the Institute of Solid State Physics, University of Latvia. He received his BSc and MSc degrees in mechanical engineering in Riga Technical University. He completed his Ph.D. in chemical physics in the University of Latvia in 2007. Later, he won a postdoctoral position in a postdoc project competition in the field of nanotribology in the Institute of Physics, University of Tartu, Estonia. After returning to Latvia, he continued his work in the Institute of Solid State Physics, University of Latvia. His research interests include synthesis and physical properties of nanomaterials and 2D layered materials. By the spring of 2021, Boris has 79 publications in the Google Scholar database with an h-index of 19.

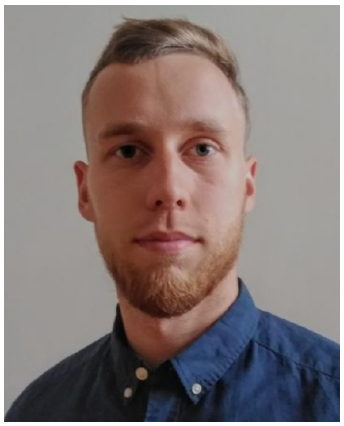

Edgars Butanovs is a senior researcher in the Thin Films Laboratory in the Institute of Solid State Physics, University of Latvia, a Research Fellow in the Institute of Technology, University of Tartu, and a lecturer in the University of Latvia. He received his BSc and MSc degrees in physics in 2014 and 2016, respectively, and completed his Ph.D. in materials physics in the University of Latvia in 2020. His research interests are related to the growth and studies of 1D and 2D nanomaterials (semiconducting nanowires and layered 2D materials), thin film deposition technologies, and optoelectronics applications. By the spring of 2021, Edgars has 16 publications in the Google Scholar database with an h-index of 5.

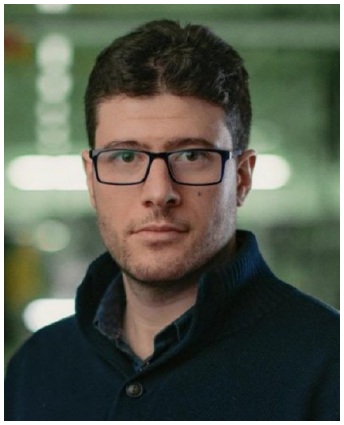

Andreas Kyritsakis (born in 1987) has a PhD in Electrical & Computer Engineering (2014, National Technical University of Athens) and a Master Degree (Diploma) in Electrical & Computer Engineering (2010, National Technical University of Athens). His research activities are focused mainly on the theoretical/computational modelling of electron emission, vacuum arcs, and nanomaterial behavior under high electric fields. At the moment, Andreas is the ERA Chair Holder of the MATTER project, leading its scientific activities. As a simulation specialist, he focuses mainly on the subgroup of multiscale nanomaterial modelling. By the spring of 2021 Andreas has 45 publications in the Google Scholar database, with an h-index of 11.

https://doi.org/10.1021/acs.cgd.1c00802
Cryst. Growth Des. 2022, 22, 871−892

Veronika Zadin is a professor of materials technology in the Institute of Technology, University of Tartu. She received her PhD in physical engineering in 2012 (University of Tartu) followed by postdoctoral research in the University of Helsinki (2012−2014). Next to the scientific work, she is involved in managing the collaboration between University of Tartu and CTF3 activities in CERN, holding there the position of Estonian group leader. Her main expertise and research interest are multiphysics finite element simulations in the nano- and microscale. Her specialization includes elastic and plastic deformations, heat and mass transport, charge transport, and interactions between the electric field and metals. By the spring of 2021, Veronika has 65 publications in the Google Scholar database, with an h-index of 15.

■ ACKNOWLEDGMENTS

The work was funded by ERA Chair MATTER from the European Union's Horizon 2020 research and innovation programme under grant agreement No 856705.

■ REFERENCES

(1) Sofiah, A. G. N.; Samykano, M.; Kadirgama, K.; Mohan, R. V.; Lah, N. A. C. Metallic nanowires: Mechanical properties − Theory and experiment *Appl. Mater. Today* **2018**, *11*, 320−37.
(2) Vlassov, S.; Polyakov, B.; Oras, S.; Vahtrus, M.; Antsov, M.; Šutka, A.; Smits, K.; Dorogin, L. M.; Lõhmus, R. Complex tribomechanical characterization of ZnO nanowires: nanomanipulations supported by FEM simulations. *Nanotechnology* **2016**, *27*, 335701.
(3) Vlassov, S.; Polyakov, B.; Vahtrus, M.; Mets, M.; Antsov, M.; Oras, S.; Tarre, A.; Arroval, T.; Lõhmus, R.; Aarik, J. Enhanced flexibility and electron-beam-controlled shape recovery in alumina-coated Au and Ag core−shell nanowires. *Nanotechnology* **2017**, *28*, 505707.
(4) Nehra, M.; Dilbaghi, N.; Marrazza, G.; Kaushik, A.; Abolhassani, R.; Mishra, Y. K.; Kim, K. H.; Kumar, S. 1D semiconductor nanowires for energy conversion, harvesting and storage applications. *Nano Energy* **2020**, *76*, 104991.
(5) Vlassov, S.; Mets, M.; Polyakov, B.; Bian, J.; Dorogin, L.; Zadin, V. Abrupt elastic-to-plastic transition in pentagonal nanowires under bending *Beilstein. Beilstein J. Nanotechnol.* **2019**, *10*, 2468−76.
(6) Antsov, M.; Polyakov, B.; Zadin, V.; Mets, M.; Oras, S.; Vahtrus, M.; Lõhmus, R.; Dorogin, L.; Vlassov, S. Mechanical characterisation of pentagonal gold nanowires in three different test configurations: A comparative study. *Micron* **2019**, *124*, 102686.
(7) Polyakov, B.; Vlassov, S.; Dorogin, L. M.; Kulis, P.; Kink, I.; Lohmus, R. The effect of substrate roughness on the static friction of CuO nanowires. *Surf. Sci.* **2012**, *606*, 1393−9.
(8) Duan, X.; Huang, Y.; Cui, Y.; Wang, J.; Lieber, C. M. Indium phosphide nanowires as building blocks for nanoscale electronic and optoelectronic devices. *Nature* **2001**, *409*, 66−9.
(9) Stern, A.; Aharon, S.; Binyamin, T.; Karmi, A.; Rotem, D.; Etgar, L.; Porath, D. Electrical Characterization of Individual Cesium Lead Halide Perovskite Nanowires Using Conductive AFM. *Adv. Mater.* **2020**, *32*, 1907812.
(10) Butanovs, E.; Vlassov, S.; Kuzmin, A.; Piskunov, S.; Butikova, J.; Polyakov, B. Fast-Response Single-Nanowire Photodetector Based on ZnO/WS_2 Core/Shell Heterostructures. *ACS Appl. Mater. Interfaces* **2018**, *10*, 13869−76.
(11) Vlassov, S.; Oras, S.; Antsov, M.; Butikova, J.; Lõhmus, R.; Polyakov, B. Low-friction nanojoint prototype. *Nanotechnology* **2018**, *29*, 195707.
(12) Rahong, S.; Yasui, T.; Kaji, N.; Baba, Y. Recent developments in nanowires for bio-applications from molecular to cellular levels. *Lab Chip* **2016**, *16*, 1126−38.
(13) Verardo, D.; Lindberg, F. W.; Anttu, N.; Niman, C. S.; Lard, M.; Dabkowska, A. P.; Nylander, T.; Månsson, A.; Prinz, C. N.; Linke, H. Nanowires for Biosensing: Lightguiding of Fluorescence as a Function of Diameter and Wavelength. *Nano Lett.* **2018**, *18*, 4796−802.
(14) Johar, M. A.; Song, H.-G.; Waseem, A.; Hassan, M. A.; Bagal, I. V.; Cho, Y.-H.; Ryu, S.-W. Universal and scalable route to fabricate GaN nanowire-based LED on amorphous substrate by MOCVD. *Appl. Mater. Today* **2020**, *19*, 100541.
(15) Thiyagu, S; Fukata, N Chapter 9 - Silicon nanowire-based solar cells. *Nanomaterials for Solar Cell Applications* **2019**, 325−348.
(16) Garnett, E. C.; Brongersma, M. L.; Cui, Y.; McGehee, M. D. Nanowire Solar Cells *Annu. Annu. Rev. Mater. Res.* **2011**, *41*, 269−95.
(17) Lan, C.; Li, C.; Wang, S.; Yin, Y.; Guo, H.; Liu, N.; Liu, Y. ZnO−WS2 heterostructures for enhanced ultra-violet photodetectors. *RSC Adv.* **2016**, *6*, 67520−4.
(18) Stokes, K.; Geaney, H.; Sheehan, M.; Borsa, D.; Ryan, K. M. Copper Silicide Nanowires as Hosts for Amorphous Si Deposition as a Route to Produce High Capacity Lithium-Ion Battery Anodes. *Nano Lett.* **2019**, *19*, 8829−35.
(19) Wei, H.; Wang, Z.; Tian, X.; Käll, M.; Xu, H. Cascaded logic gates in nanophotonic plasmon networks. *Nat. Commun.* **2011**, *2*, 387.
(20) Huang, Y.; Duan, X.; Cui, Y.; Lauhon, L. J.; Kim, K.-H.; Lieber, C. M. Logic Gates and Computation from Assembled Nanowire Building Blocks. *Science* **2001**, *294*, 1313−7.
(21) Huo, N.; Yang, S.; Wei, Z.; Li, S.-S.; Xia, J.-B.; Li, J. Photoresponsive and Gas Sensing Field-Effect Transistors based on Multilayer WS_2 Nanoflakes. *Sci. Rep.* **2015**, *4*, 5209.
(22) Hu, X. F.; Li, S. J.; Wang, J.; Jiang, Z. M.; Yang, X. J. Investigating Size-Dependent Conductive Properties on Individual Si Nanowires. *Nanoscale Res. Lett.* **2020**, *15*, 52.
(23) Nam, C.-Y.; Jaroenapibal, P.; Tham, D.; Luzzi, D. E.; Evoy, S.; Fischer, J. E. Diameter-Dependent Electromechanical Properties of GaN Nanowires. *Nano Lett.* **2006**, *6*, 153−8.
(24) Yorikawa, H.; Uchida, H.; Muramatsu, S. Energy gap of nanoscale Si rods. *J. Appl. Phys.* **1996**, *79*, 3619−21.
(25) Roy, A.; Mead, J.; Wang, S.; Huang, H. Effects of surface defects on the mechanical properties of ZnO nanowires. *Sci. Rep.* **2017**, *7*, 9547.
(26) Shin, N.; Chi, M.; Filler, M. A. Sidewall Morphology-Dependent Formation of Multiple Twins in Si Nanowires. *ACS Nano* **2013**, *7*, 8206−13.
(27) Arbiol, J.; Fontcuberta i Morral, A.; Estradé, S.; Peiró, F.; Kalache, B.; Roca i Cabarrocas, P.; Morante, J. R. Influence of the (111) twinning on the formation of diamond cubic/diamond hexagonal heterostructures in Cu-catalyzed Si nanowires. *J. Appl. Phys.* **2008**, *104*, No. 064312.
(28) Sosnin, I. M.; Vlassov, S.; Akimov, E. G.; Agenkov, V. I.; Dorogin, L. M. Transparent ZnO-coated polydimethylsiloxane-based material for photocatalytic purification applications. *J. Coat. Technol. Res.* **2020**, *17*, 573−9.
(29) Murphy, K. F.; Piccione, B.; Zanjani, M. B.; Lukes, J. R.; Gianola, D. S. Strain- and Defect-Mediated Thermal Conductivity in Silicon Nanowires. *Nano Lett.* **2014**, *14*, 3785−92.
(30) Barth, S.; Boland, J. J.; Holmes, J. D. Defect Transfer from Nanoparticles to Nanowires. *Nano Lett.* **2011**, *11*, 1550−5.
(31) Shin, N.; Chi, M.; Howe, J. Y.; Filler, M. A. Rational Defect Introduction in Silicon Nanowires. *Nano Lett.* **2013**, *13*, 1928−33.
(32) Ra, H.-W.; Khan, R.; Kim, J. T.; Kang, B. R.; Bai, K. H.; Im, Y. H. Effects of surface modification of the individual ZnO nanowire with oxygen plasma treatment. *Mater. Lett.* **2009**, *63*, 2516−9.

https://doi.org/10.1021/acs.cgd.1c00802
Cryst. Growth Des. 2022, 22, 871−892

(33) Muhammad, B. L.; Cummings, F. Nitrogen plasma treatment of ZnO and TiO2 nanowire arrays for polymer photovoltaic applications. *Surf. Interfaces* **2019**, *17*, 100382.
(34) Yang, B.; Liu, B.; Wang, Y.; Zhuang, H.; Liu, Q.; Yuan, F.; Jiang, X. Zn-dopant dependent defect evolution in GaN nanowires. *Nanoscale* **2015**, *7*, 16237−45.
(35) Ghosh, S.; Gopal Khan, G.; Varma, S.; Mandal, K. Influence of Li-N and Li-F co-doping on defect-induced intrinsic ferromagnetic and photoluminescence properties of arrays of ZnO nanowires. *J. Appl. Phys.* **2012**, *112*, No. 043910.
(36) Narayanan, S.; Cheng, G.; Zeng, Z.; Zhu, Y.; Zhu, T. Strain Hardening and Size Effect in Five-fold Twinned Ag Nanowires. *Nano Lett.* **2015**, *15*, 4037−44.
(37) Li, Y.; Wang, Y.; Ryu, S.; Marshall, A. F.; Cai, W.; McIntyre, P. C. Spontaneous, Defect-Free Kinking via Capillary Instability during Vapor−Liquid−Solid Nanowire Growth. *Nano Lett.* **2016**, *16*, 1713−8.
(38) Jiang, J.-W.; Yang, N.; Wang, B.-S.; Rabczuk, T. Modulation of Thermal Conductivity in Kinked Silicon Nanowires: Phonon Interchanging and Pinching Effects. *Nano Lett.* **2013**, *13*, 1670−4.
(39) Cook, B. G.; Varga, K. Conductance of kinked nanowires. *Appl. Phys. Lett.* **2011**, *98*, 052104.
(40) Zhao, Y.; Yang, L.; Liu, C.; Zhang, Q.; Chen, Y.; Yang, J.; Li, D. Kink effects on thermal transport in silicon nanowires. *Int. J. Heat Mass Transfer* **2019**, *137*, 573−8.
(41) Tian, B.; Xie, P.; Kempa, T. J.; Bell, D. C.; Lieber, C. M. Single crystalline kinked semiconductor nanowire superstructures. *Nat. Nanotechnol.* **2009**, *4*, 824−9.
(42) Fortuna, S. A.; Li, X. Metal-catalyzed semiconductor nanowires: a review on the control of growth directions. *Semicond. Sci. Technol.* **2010**, *25*, No. 024005.
(43) Ross, F. M. Controlling nanowire structures through real time growth studies. *Rep. Prog. Phys.* **2010**, *73*, 114501.
(44) Tian, B.; Cohen-Karni, T.; Qing, Q.; Duan, X.; Xie, P.; Lieber, C. M. Three-Dimensional, Flexible Nanoscale Field-Effect Transistors as Localized Bioprobes. *Science* **2010**, *329*, 830−4.
(45) Xu, L.; Jiang, Z.; Qing, Q.; Mai, L.; Zhang, Q.; Lieber, C. M. Design and Synthesis of Diverse Functional Kinked Nanowire Structures for Nanoelectronic Bioprobes. *Nano Lett.* **2013**, *13*, 746−51.
(46) Barth, S.; Hernandez-Ramirez, F.; Holmes, J. D.; Romano-Rodriguez, A. Synthesis and applications of one-dimensional semiconductors. *Prog. Mater. Sci.* **2010**, *55*, 563−627.
(47) Lugstein, A.; Steinmair, M.; Hyun, Y. J.; Hauer, G.; Pongratz, P.; Bertagnolli, E. Pressure-Induced Orientation Control of the Growth of Epitaxial Silicon Nanowires. *Nano Lett.* **2008**, *8*, 2310−4.
(48) Hyun, Y.-J.; Lugstein, A.; Steinmair, M.; Bertagnolli, E.; Pongratz, P. Orientation specific synthesis of kinked silicon nanowires grown by the vapour−liquid−solid mechanism. *Nanotechnology* **2009**, *20*, 125606.
(49) Geaney, H.; Dickinson, C.; Weng, W.; Kiely, C. J.; Barrett, C. A.; Gunning, R. D.; Ryan, K. M. Role of Defects and Growth Directions in the Formation of Periodically Twinned and Kinked Unseeded Germanium Nanowires. *Cryst. Growth Des.* **2011**, *11*, 3266−72.
(50) Kim, J. H.; Moon, S. R.; Yoon, H. S.; Jung, J. H.; Kim, Y.; Chen, Z. G.; Zou, J.; Choi, D. Y.; Joyce, H. J.; Gao, Q.; Tan, H. H.; Jagadish, C. Taper-Free and Vertically Oriented Ge Nanowires on Ge/Si Substrates Grown by a Two-Temperature Process. *Cryst. Growth Des.* **2012**, *12*, 135−41.
(51) Wu, Z. H.; Mei, X.; Kim, D.; Blumin, M.; Ruda, H. E.; Liu, J. Q.; Kavanagh, K. L. Growth, branching, and kinking of molecular-beam epitaxial ⟨110⟩ GaAs nanowires. *Appl. Phys. Lett.* **2003**, *83*, 3368−70.
(52) Peng, H.; Meister, S.; Chan, C. K.; Zhang, X. F.; Cui, Y. Morphology Control of Layer-Structured Gallium Selenide Nanowires. *Nano Lett.* **2007**, *7*, 199−203.
(53) Jiang, Z.; Qing, Q.; Xie, P.; Gao, R.; Lieber, C. M. Kinked p−n Junction Nanowire Probes for High Spatial Resolution Sensing and Intracellular Recording. *Nano Lett.* **2012**, *12*, 1711−6.
(54) Jiang, J.-W.; Zhao, J.-H.; Rabczuk, T. Size-sensitive Young's modulus of kinked silicon nanowires. *Nanotechnology* **2013**, *24*, 185702.
(55) Jiang, J.-W.; Rabczuk, T. Mechanical oscillation of kinked silicon nanowires: A natural nanoscale spring. *Appl. Phys. Lett.* **2013**, *102*, 123104.
(56) Hillerich, K.; Dick, K. A.; Wen, C.-Y.; Reuter, M. C.; Kodambaka, S.; Ross, F. M. Strategies To Control Morphology in Hybrid Group III−V/Group IV Heterostructure Nanowires. *Nano Lett.* **2013**, *13*, 903−8.
(57) Dick, K. A.; Kodambaka, S.; Reuter, M. C.; Deppert, K.; Samuelson, L.; Seifert, W.; Wallenberg, L. R.; Ross, F. M. The Morphology of Axial and Branched Nanowire Heterostructures. *Nano Lett.* **2007**, *7*, 1817−22.
(58) Dayeh, S. A.; Wang, J.; Li, N.; Huang, J. Y.; Gin, A. V.; Picraux, S. T. Growth, Defect Formation, and Morphology Control of Germanium−Silicon Semiconductor Nanowire Heterostructures. *Nano Lett.* **2011**, *11*, 4200−6.
(59) Paladugu, M.; Zou, J.; Guo, Y.-N.; Auchterlonie, G. J.; Joyce, H. J.; Gao, Q.; Hoe Tan, H.; Jagadish, C.; Kim, Y. Novel Growth Phenomena Observed in Axial InAs/GaAs Nanowire Heterostructures. *Small* **2007**, *3*, 1873.
(60) He, Z.; Nguyen, H. T.; Duc Toan, L.; Pribat, D. A detailed study of kinking in indium-catalyzed silicon nanowires. *CrystEngComm* **2015**, *17*, 6286.
(61) McIntyre, P. C.; Fontcuberta i Morral, I. Semiconductor nanowires: to grow or not to grow? *Mater. Today Nano* **2020**, *9*, 100058.
(62) Thombare, S. V.; Marshall, A. F.; McIntyre, P. C. Size effects in vapor-solid-solid Ge nanowire growth with a Ni-based catalyst. *J. Appl. Phys.* **2012**, *112*, No. 054325.
(63) Fahlvik Svensson, S.; Jeppesen, S.; Thelander, C.; Samuelson, L.; Linke, H.; Dick, K. A. Control and understanding of kink formation in InAs−InP heterostructure nanowires. *Nanotechnology* **2013**, *24*, 345601.
(64) Madras, P.; Dailey, E.; Drucker, J. Kinetically Induced Kinking of Vapor−Liquid−Solid Grown Epitaxial Si Nanowires. *Nano Lett.* **2009**, *9*, 3826−30.
(65) Sun, Z.; Seidman, D. N.; Lauhon, L. J. Nanowire Kinking Modulates Doping Profiles by Reshaping the Liquid−Solid Growth Interface. *Nano Lett.* **2017**, *17*, 4518−25.
(66) Yuan, X.; Caroff, P.; Wong-Leung, J.; Fu, L.; Tan, H. H.; Jagadish, C. Tunable Polarity in a III−V Nanowire by Droplet Wetting and Surface Energy Engineering. *Adv. Mater.* **2015**, *27*, 6096−103.
(67) Shin, N.; Chi, M.; Filler, M. A. Interplay between Defect Propagation and Surface Hydrogen in Silicon Nanowire Kinking Superstructures. *ACS Nano* **2014**, *8*, 3829−35.
(68) Schmidt, V.; Senz, S.; Gösele, U. Diameter-Dependent Growth Direction of Epitaxial Silicon Nanowires. *Nano Lett.* **2005**, *5*, 931−5.
(69) Wu, Y.; Cui, Y.; Huynh, L.; Barrelet, C. J.; Bell, D. C.; Lieber, C. M. Controlled Growth and Structures of Molecular-Scale Silicon Nanowires. *Nano Lett.* **2004**, *4*, 433−6.
(70) Wen, C.-Y.; Reuter, M. C.; Tersoff, J.; Stach, E. A.; Ross, F. M. Structure, Growth Kinetics, and Ledge Flow during Vapor−Solid−Solid Growth of Copper-Catalyzed Silicon Nanowires. *Nano Lett.* **2010**, *10*, 514−9.
(71) Wang, Y.; Schmidt, V.; Senz, S.; Gösele, U. Epitaxial growth of silicon nanowires using an aluminium catalyst. *Nat. Nanotechnol.* **2006**, *1*, 186−9.
(72) Wacaser, B. A.; Reuter, M. C.; Khayyat, M. M.; Wen, C.-Y.; Haight, R.; Guha, S.; Ross, F. M. Growth System, Structure, and Doping of Aluminum-Seeded Epitaxial Silicon Nanowires. *Nano Lett.* **2009**, *9*, 3296−301.
(73) Hainey, M.; Eichfeld, S. M.; Shen, H.; Yim, J.; Black, M. R.; Redwing, J. M. Aluminum-Catalyzed Growth of ⟨110⟩ Silicon Nanowires. *J. Electron. Mater.* **2015**, *44*, 1332−7.
(74) Conesa-Boj, S.; Zardo, I.; Estradé, S.; Wei, L.; Jean Alet, P.; Roca i Cabarrocas, P.; Morante, J. R.; Peiró, F.; Morral, A F i; Arbiol, J. Defect Formation in Ga-Catalyzed Silicon Nanowires. *Cryst. Growth Des.* **2010**, *10*, 1534−43.

https://doi.org/10.1021/acs.cgd.1c00802
Cryst. Growth Des. 2022, 22, 871−892

(75) Sharma, S.; Sunkara, M. K. Direct synthesis of single-crystalline silicon nanowires using molten gallium and silane plasma. *Nanotechnology* **2004**, *15*, 130−4.
(76) Wang, Z. W.; Li, Z. Y. Structures and Energetics of Indium-Catalyzed Silicon Nanowires. *Nano Lett.* **2009**, *9*, 1467−71.
(77) Schwarz, K. W.; Tersoff, J.; Kodambaka, S.; Chou, Y.-C.; Ross, F. M. Geometrical Frustration in Nanowire Growth. *Phys. Rev. Lett.* **2011**, *107*, 265502.
(78) Hughes, W. L.; Wang, Z. L. Formation of Piezoelectric Single-Crystal Nanorings and Nanobows. *J. Am. Chem. Soc.* **2004**, *126*, 6703−9.
(79) Shen, G.; Liang, B.; Wang, X.; Chen, P.-C.; Zhou, C. Indium Oxide Nanospirals Made of Kinked Nanowires. *ACS Nano* **2011**, *5*, 2155−61.
(80) Zhou, X. T.; Sham, T. K.; Shan, Y. Y.; Duan, X. F.; Lee, S. T.; Rosenberg, R. A. One-dimensional zigzag gallium nitride nanostructures. *J. Appl. Phys.* **2005**, *97*, 104315.
(81) Panda, S. K.; Datta, A.; Sinha, G.; Chaudhuri, S.; Chavan, P. G.; Patil, S. S.; More, M. A.; Joag, D. S. Synthesis of Well-Crystalline GaS Nanobelts and Their Unique Field Emission Behavior. *J. Phys. Chem. C* **2008**, *112*, 6240−4.
(82) Hong, W.-K.; Sohn, J. I.; Hwang, D.-K.; Kwon, S.-S.; Jo, G.; Song, S.; Kim, S.-M.; Ko, H.-J.; Park, S.-J.; Welland, M. E.; Lee, T. Tunable Electronic Transport Characteristics of Surface-Architecture-Controlled ZnO Nanowire Field Effect Transistors. *Nano Lett.* **2008**, *8*, 950−6.
(83) Potts, H.; Morgan, N. P.; Tütüncüoglu, G.; Friedl, M.; Morral, A F i Tuning growth direction of catalyst-free InAs(Sb) nanowires with indium droplets. *Nanotechnology* **2017**, *28*, No. 054001.
(84) Sivaram, S. V.; Hui, H. Y.; de la Mata, M.; Arbiol, J.; Filler, M. A. Surface Hydrogen Enables Subeutectic Vapor−Liquid−Solid Semiconductor Nanowire Growth. *Nano Lett.* **2016**, *16*, 6717−23.
(85) Kodambaka, S.; Tersoff, J.; Reuter, M. C.; Ross, F. M. Germanium Nanowire Growth Below the Eutectic Temperature. *Science* **2007**, *316*, 729−32.
(86) Kim, J. H.; Moon, S. R.; Kim, Y.; Chen, Z. G.; Zou, J.; Choi, D. Y.; Joyce, H. J.; Gao, Q.; Tan, H. H.; Jagadish, C. Taper-free and kinked germanium nanowires grown on silicon via purging and the two-temperature process. *Nanotechnology* **2012**, *23*, 115603.
(87) Li, Z.; Kurtulus, Ö; Fu, N.; Wang, Z.; Kornowski, A.; Pietsch, U.; Mews, A. Controlled Synthesis of CdSe Nanowires by Solution−Liquid−Solid Method. *Adv. Funct. Mater.* **2009**, *19*, 3650−61.
(88) Schmidt, V.; Senz, S.; Gösele, U. The shape of epitaxially grown silicon nanowires and the influence of line tension. *Appl. Phys. A: Mater. Sci. Process.* **2005**, *80*, 445−50.
(89) Ghisalberti, L.; Potts, H.; Friedl, M.; Zamani, M.; Güniat, L.; Tütüncüoglu, G.; Carter, W. C.; Morral, A F i Questioning liquid droplet stability on nanowire tips: from theory to experiment. *Nanotechnology* **2019**, *30*, 285604.
(90) Schwarz, K. W.; Tersoff, J. From Droplets to Nanowires: Dynamics of Vapor-Liquid-Solid Growth. *Phys. Rev. Lett.* **2009**, *102*, 206101.
(91) Schwarz, K. W.; Tersoff, J. Elementary Processes in Nanowire Growth. *Nano Lett.* **2011**, *11*, 316−20.
(92) Chen, Y.; Zhang, C.; Li, L.; Tuan, C.-C.; Chen, X.; Gao, J.; He, Y.; Wong, C.-P. Effects of Defects on the Mechanical Properties of Kinked Silicon Nanowires. *Nanoscale Res. Lett.* **2017**, *12*, 185.
(93) Westwater, J.; Gosain, D. P.; Tomiya, S.; Usui, S.; Ruda, H. Growth of silicon nanowires via gold/silane vapor−liquid−solid reaction. *J. Vac. Sci. Technol., B: Microelectron. Process. Phenom.* **1997**, *15*, 554−7.
(94) Adhikari, H.; Marshall, A. F.; Chidsey, C. E. D.; McIntyre, P. C. Germanium Nanowire Epitaxy: Shape and Orientation Control. *Nano Lett.* **2006**, *6*, 318−23.
(95) Hiruma, K.; Yazawa, M.; Haraguchi, K.; Ogawa, K.; Katsuyama, T.; Koguchi, M.; Kakibayashi, H. GaAs free-standing quantum-size wires. *J. Appl. Phys.* **1993**, *74*, 3162−71.
(96) Borgström, M.; Deppert, K.; Samuelson, L.; Seifert, W. Size- and shape-controlled GaAs nano-whiskers grown by MOVPE: a growth study. *J. Cryst. Growth* **2004**, *260*, 18−22.
(97) Hiruma, K.; Murakoshi, H.; Yazawa, M.; Katsuyama, T. Self-organized growth of GaAsInAs heterostructure nanocylinders by organometallic vapor phase epitaxy. *J. Cryst. Growth* **1996**, *163*, 226−31.
(98) Kim, Y.; Joyce, H. J.; Gao, Q.; Tan, H. H.; Jagadish, C.; Paladugu, M.; Zou, J.; Suvorova, A. A. Influence of Nanowire Density on the Shape and Optical Properties of Ternary InGaAs Nanowires. *Nano Lett.* **2006**, *6*, 599−604.
(99) Johansson, J.; Karlsson, L. S.; Svensson, C. P. T.; Martensson, T.; Wacaser, B. A.; Deppert, K.; Samuelson, L.; Seifert, W. Structural properties of ⟨111⟩B -oriented III−V nanowires. *Nat. Mater.* **2006**, *5*, 574.
(100) Wagner, R. S.; Ooherty, C. J. Mechanism of Branching and Kinking during VLS Crystal Growth. *J. Electrochem. Soc.* **1968**, *115*, 93.
(101) Song, M. S.; Jung, J. H.; Kim, Y.; Wang, Y.; Zou, J.; Joyce, H. J.; Gao, Q.; Tan, H. H.; Jagadish, C. Vertically standing Ge nanowires on GaAs(110) substrates. *Nanotechnology* **2008**, *19*, 125602.
(102) Schmid, H.; Björk, M. T.; Knoch, J.; Riel, H.; Riess, W.; Rice, P.; Topuria, T. Patterned epitaxial vapor-liquid-solid growth of silicon nanowires on Si(111) using silane. *J. Appl. Phys.* **2008**, *103*, No. 024304.
(103) Shin, N.; Filler, M. A. Controlling Silicon Nanowire Growth Direction via Surface Chemistry. *Nano Lett.* **2012**, *12*, 2865−70.
(104) Musin, I. R.; Filler, M. A. Chemical Control of Semiconductor Nanowire Kinking and Superstructure. *Nano Lett.* **2012**, *12*, 3363−8.
(105) Dailey, E.; Drucker, J. Seedless" vapor-liquid-solid growth of Si and Ge nanowires: The origin of bimodal diameter distributions. *J. Appl. Phys.* **2009**, *105*, No. 064317.
(106) Xie, P.; Hu, Y.; Fang, Y.; Huang, J.; Lieber, C. M. Diameter-dependent dopant location in silicon and germanium nanowires. *Proc. Natl. Acad. Sci. U. S. A.* **2009**, *106*, 15254−8.
(107) Perea, D. E.; Hemesath, E. R.; Schwalbach, E. J.; Lensch-Falk, J. L.; Voorhees, P. W.; Lauhon, L. J. Direct measurement of dopant distribution in an individual vapour−liquid−solid nanowire. *Nat. Nanotechnol.* **2009**, *4*, 315−9.
(108) Jagannathan, H.; Deal, M.; Nishi, Y.; Woodruff, J.; Chidsey, C.; McIntyre, P. C. Nature of germanium nanowire heteroepitaxy on silicon substrates. *J. Appl. Phys.* **2006**, *100*, No. 024318.
(109) Kodambaka, S.; Hannon, J. B.; Tromp, R. M.; Ross, F. M. Control of Si Nanowire Growth by Oxygen. *Nano Lett.* **2006**, *6*, 1292−6.
(110) Joyce, H. J.; Gao, Q.; Tan, H. H.; Jagadish, C.; Kim, Y.; Fickenscher, M. A.; Perera, S.; Hoang, T. B.; Smith, L. M.; Jackson, H. E.; Yarrison-Rice, J. M.; Zhang, X.; Zou, J. High Purity GaAs Nanowires Free of Planar Defects: Growth and Characterization. *Adv. Funct. Mater.* **2008**, *18*, 3794−800.
(111) Anon Nanotectonics | COMC.
(112) Wang, J.; Plissard, S. R.; Verheijen, M. A.; Feiner, L.-F.; Cavalli, A.; Bakkers, E. P. A. M. Reversible Switching of InP Nanowire Growth Direction by Catalyst Engineering. *Nano Lett.* **2013**, *13*, 3802−6.
(113) Zhang, Z.; Zheng, K.; Lu, Z.-Y.; Chen, P.-P.; Lu, W.; Zou, J. Catalyst Orientation-Induced Growth of Defect-Free Zinc-Blende Structured ⟨00$\bar{1}$⟩ InAs Nanowires. *Nano Lett.* **2015**, *15*, 876−82.
(114) Verheijen, M. A.; Immink, G.; de Smet, T.; Borgström, M. T.; Bakkers, E. P. A. M. Growth Kinetics of Heterostructured GaP−GaAs Nanowires. *J. Am. Chem. Soc.* **2006**, *128*, 1353−9.
(115) Dayeh, S. A.; Yu, E. T.; Wang, D. III−V Nanowire Growth Mechanism: V/III Ratio and Temperature Effects. *Nano Lett.* **2007**, *7*, 2486−90.
(116) Chen, Y.; Li, L.; Zhang, C.; Tuan, C.-C.; Chen, X.; Gao, J.; Wong, C.-P. Controlling Kink Geometry in Nanowires Fabricated by Alternating Metal-Assisted Chemical Etching. *Nano Lett.* **2017**, *17*, 1014−9.
(117) Sandu, G.; Avila Osses, J.; Luciano, M.; Caina, D.; Stopin, A.; Bonifazi, D.; Gohy, J.-F.; Silhanek, A.; Florea, I.; Bahri, M.; Ersen, O.; Leclère, P.; Gabriele, S.; Vlad, A.; Melinte, S. Kinked Silicon Nanowires:

https://doi.org/10.1021/acs.cgd.1c00802
Cryst. Growth Des. 2022, 22, 871−892

Superstructures by Metal-Assisted Chemical Etching. *Nano Lett.* **2019**, *19*, 7681−90.
(118) Joyce, H. J.; Gao, Q.; Tan, H. H.; Jagadish, C.; Kim, Y.; Zhang, X.; Guo, Y.; Zou, J. Twin-Free Uniform Epitaxial GaAs Nanowires Grown by a Two-Temperature Process. *Nano Lett.* **2007**, *7*, 921−6.
(119) Dick, K. A.; Caroff, P. Metal-seeded growth of III−V semiconductor nanowires: towards gold-free synthesis. *Nanoscale* **2014**, *6*, 3006−21.
(120) Jing, Y.; Zhang, C.; Liu, Y.; Guo, L.; Meng, Q. Mechanical properties of kinked silicon nanowires. *Phys. B* **2015**, *462*, 59−63.
(121) Jiang, J.-W. Intrinsic twisting instability of kinked silicon nanowires for intracellular recording. *Phys. Chem. Chem. Phys.* **2015**, *17*, 28515−24.
(122) Zhang, Q.; Cui, Z.; Wei, Z.; Chang, S. Y.; Yang, L.; Zhao, Y.; Yang, Y.; Guan, Z.; Jiang, Y.; Fowlkes, J.; Yang, J.; Xu, D.; Chen, Y.; Xu, T. T.; Li, D. Defect Facilitated Phonon Transport through Kinks in Boron Carbide Nanowires. *Nano Lett.* **2017**, *17*, 3550−5.
(123) Gan, L.; Liao, M.; Li, H.; Ma, Y.; Zhai, T. Geometry-induced high performance ultraviolet photodetectors in kinked SnO2 nanowires. *J. Mater. Chem. C* **2015**, *3*, 8300−6.
(124) Islam, M. S.; Sharma, S.; Kamins, T. I.; Williams, R. S. Ultrahigh-density silicon nanobridges formed between two vertical silicon surfaces. *Nanotechnology* **2004**, *15*, L5.

The Institute of Solid State Physics, University of Latvia, as a center of excellence, has received funding from the European Union's Horizon 2020 Framework Programme H2020-WIDESPREAD-01-2016-2017-TeamingPhase2 under grant agreement no. 739508, project CAMART2.

https://doi.org/10.1021/acs.cgd.1c00802
Cryst. Growth Des. 2022, 22, 871−892